Molecular Neurobiology (2026) 63:383
https://doi.org/10.1007/s12035-026-05700-7

RESEARCH

Mitochondrial Dynamics-Related Gene Regulation by Epigenetic Suppression of GCN5 Exerts Neuroprotective Effects in Rotenone-Induced Parkinson's Disease Model

Gökçe Ceren Kuşçu[1] · Ezgi Tut[2] · Çevik Gürel[3] · Aylin Buhur[4] · Özgün Selim Germiyan[5] · Çığır Biray Avcı[6] · Cem Güler[7] · Ebru Şancı[7] · Nefise Ülkü Karabay Yavaşoğlu[7] · Altuğ Yavaşoğlu[1]

Received: 26 October 2025 / Accepted: 15 January 2026

Abstract

Parkinson's disease (PD) is a progressive neurodegenerative disorder characterized by dopaminergic neuron loss and mitochondrial dysfunction. Recent studies implicate the histone acetyltransferase GCN5 in regulating mitochondrial homeostasis and oxidative stress. This study investigated the therapeutic potential of GCN5 silencing via systemically administered siRNA-loaded niosomes in a rotenone-induced rat model of PD. Niosomes were prepared using the thin-film hydration method, and the most effective siRNA sequence was selected through real time quantitative PCR (RT-qPCR) and immunofluorescence in primary mesencephalic neurons. Adult male rats were divided into four groups (n = 24/group), and PD was induced with rotenone (2 mg/kg/day, s.c., for 35 days). Behavioral assessments, biochemical analyses, IVIS imaging, histopathology, immunohistochemistry, and RT-qPCR were conducted. IVIS confirmed brain accumulation of siRNA–niosomes within 3–5 h post-injection. GCN5 siRNA treatment significantly improved locomotor activity ($p < 0.05$), decreased MDA levels ($p < 0.05$), and restored SOD and dopamine levels ($p < 0.05$). Molecular findings showed decreased GCN5 and mitochondrial fission-related gene Drp-1 expression, increased expression of mitophagy and biogenesis markers (↑Parkin, ↑PINK1, ↑Mfn2, ↑PGC-1α), elevated TH expression, and reduced α-synuclein accumulation. Histological analysis revealed preserved midbrain cytoarchitecture and reduced neuronal damage. In conclusion, these findings highlight that epigenetic silencing of GCN5 via siRNA-loaded niosomal delivery provides neuroprotection in PD by modulating the expression of genes involved in mitochondrial dynamics, offering preclinical support for its development as a novel therapeutic strategy.

Keywords GCN5 · Mitochondrial dynamics · Niosome · Parkinson's disease · SiRNA delivery

Introduction

Parkinson's disease (PD) is the second most common chronic neurodegenerative disorder, characterized by motor symptoms such as tremor, postural instability, bradykinesia, and rigidity, resulting from the loss of dopaminergic neurons and the presence of Lewy Bodies (LB) in the *substantia nigra pars compacta* (SNpc) [1, 2]. Although the etiopathogenesis of PD has not yet been fully elucidated, accumulating scientific evidence suggests that oxidative stress and neuroinflammation, resulting from mitochondrial dysfunction, directly or indirectly induce dopaminergic neuron death and lead to the formation of LB [1, 3]. In fact, mutations and/or dysfunctions in the Parkin, PINK1, LRRK2, DJ-1, and SNCA genes, which are involved in mitochondrial homeostasis and biogenesis, have been shown in preclinical studies and postmortem brain analyses to cause α-synuclein

✉ Gökçe Ceren Kuşçu
gokce.ceren.kuscu@gmail.com

1 Department of Histology and Embryology, Faculty of Medicine, Ege University, İzmir, Turkey

2 Department of Nuclear Application, Institute of Nuclear Sciences, Ege University, İzmir, Turkey

3 Department of Histology and Embryology, Faculty of Medicine, Harran University, Şanlıurfa, Turkey

4 Department of Basic Sciences, Faculty of Dentistry, İstanbul Galata University, Istanbul, Turkey

5 Department of Stem Cell, Institute of Health Sciences, Ege University, İzmir, Turkey

6 Department of Medical Biology, Faculty of Medicine, Ege University, İzmir, Turkey

7 Department of General Biology, Faculty of Science, Ege University, İzmir, Turkey

Published online: 21 January 2026

(α-syn) accumulation and oxidative stress in both idiopathic and genetic forms of PD, thus undeniably highlighting the role of mitochondrial dysfunction in PD pathogenesis [4, 5]. Therefore, elucidating how the complex mechanism between mitochondrial biogenesis and mitochondrial quality control becomes dysfunctional in PD is crucial for developing effective therapeutic strategies for this disease [6].

Histone acetylation is a critical epigenetic modification that plays a central role in the regulation of gene expression through the rearrangement of chromatin architecture by the antagonistic histone acetyltransferases (HATs) and histone deacetyltransferases (HDACs) enzymes [7, 8]. This modification acts as a master regulator of numerous molecular processes in mammals, including cellular signaling, DNA replication, cytoskeletal organization, DNA damage repair, autophagy, and the cell cycle [9]. Having vital regulatory roles under physiological conditions, this epigenetic mechanism is also known to be a key contributor to the pathobiology of diverse diseases, including cancer and PD [10]. In fact, analyses conducted on postmortem brain tissue from PD patients indicate an increase in H3 acetylation in the primary motor cortex [11]. Also, it has been reported that α-syn aggregates tend to bind to H3 histones excessively acetylated by HATs, and that this interaction causes oxidative stress induced by mitochondrial dysfunction, thereby triggering dopaminergic neuronal damage [12, 13]. Moreover, the demonstration that HAT inhibitors such as garcinol, anacardic acid, and curcumin exert a therapeutic effect on L-DOPA-induced dyskinesia [14] suggests that therapeutic agents modulating the acetylation process carried out by HATs may hold promise for the treatment of PD.

General Control Non-Derepressible 5 (GCN5) is the first identified enzyme with intrinsic HAT activity capable of linking histone acetylation to transcriptional regulation in mammals [15]. This HAT, encoded by the KAT2 gene in mammals, also has a major effect on cellular energy metabolism through acetylation of molecules involved in energy metabolism, such as peroxisome proliferator-activated receptor γ coactivator 1-α (PGC-1α) [16]. Additionally, GCN5 plays a key role in the regulation of mitochondrial biogenesis and mitophagy pathways, and GCN5 mutation results in increased mitochondrial biogenesis and mitophagy [16, 17]. Moreover, it also demonstrated that GCN5 inhibition protects neurons against huntingtin-induced neurodegeneration by causing an increase in PGC-1α activity [18]. Furthermore, the GCN5 inhibitor MB-3 has been shown to protect neurons from 1-Methyl-4-phenylpyridinium (MPP^+) toxicity in an experimental PD model using the SH-SY5Y cell line [19]. Based on this information, it can be proposed that inhibition of GCN5 activity, which has a significant impact on mitochondria and cellular energy through the acetylation of molecules like PGC-1α, may exert a protective effect in neurodegenerative diseases such as PD.

RNA interference (RNAi) is gaining increasing recognition as an epigenetic therapeutic modality due to its unique ability to selectively suppress the expression of pathological genes at the post-transcriptional level [20]. Particularly in the context of neurodegenerative diseases such as PD, RNAi-based interventions hold promise for attenuating molecular dysregulations that underlie disease progression, including chronic neuroinflammation, oxidative stress, and proteostasis disruption [21, 22]. Despite its therapeutic potential, one of the major hurdles in RNAi application to central nervous system (CNS) disorders lies in the effective and non-toxic delivery of small interfering RNAs (siRNAs) across the blood–brain barrier (BBB) [23]. To address this challenge, niosomes—nano-sized vesicles formed from non-ionic surfactants and cholesterol—have emerged as viable carriers for gene-silencing agents. These nanocarriers, which typically range in diameter from 100 to 300 nm, can encapsulate both hydrophilic and lipophilic molecules and can be functionally modified with surface ligands or polymers (e.g., PEG) to improve their targeting specificity, circulation time, and cellular uptake [24]. Their physicochemical characteristics, particularly their compatibility with neuronal membranes and low immunogenicity, make niosomes particularly suitable for CNS-targeted delivery systems [23, 25]. In vivo studies have already demonstrated the clinical relevance of niosomal formulations in PD models. For instance, a study involving intranasal administration of a quercetin-loaded niosomal gel in a haloperidol-induced PD rat model reported significant restoration of motor coordination, enhanced dopaminergic neuronal survival, and reduction in oxidative markers compared to conventional delivery methods [26]. Similarly, pramipexole-loaded PEGylated niosomes showed comparable behavioral improvements to oral administration, despite requiring a substantially lower dose, emphasizing the dose-sparing advantage of nanocarrier-mediated delivery [27]. Taken together, these findings underscore the therapeutic utility of niosomal nanocarriers in RNAi-based gene silencing strategies for PD. Their ability to protect siRNAs from nuclease degradation, facilitate BBB penetration, and ensure targeted delivery to affected brain regions makes them promising vehicles in the development of next-generation gene therapies.

In this context, the aim of this study is to investigate the effects of GCN5 gene silencing via small interfering RNA (siRNA) loaded niosomes on mitophagy and mitochondrial biogenesis in an experimental PD model, utilizing behavioral assays, histological analysis, biochemical assessments, and molecular investigations.

Materials and Methods

Ethics Statement

All experimental procedures were performed in compliance with the guidelines outlined in the Guide for the Care and Use of Laboratory Animals published by the

National Institutes of Health. The experimental protocol was reviewed and approved by Ege University Animal Experimentation Local Ethics Committee (Approval Number: 2021–040; Approval Date: June 23, 2021).

Primary Culture of Mesencephalic Dopaminergic Neurons

The procedure for isolating and culturing primary dopaminergic neurons from the mesencephalon was adapted from the method outlined by Weinert et al. [28]. Briefly, time-pregnant Sprague–Dawley (SD) rats at embryonic day 14.5 (E14.5) were procured from the Ege University Laboratory Animal Research and Application Center. Following anesthesia with CO_2 and euthanasia via cervical dislocation, the abdominal surface was disinfected using 70% ethanol. A midline incision was made to expose the uterine horns, which were subsequently excised and placed into petri dishes containing ice-cold Hank's Balanced Salt Solution (HBSS) (HBSS-3A; Capricorn, Ebsdorfergrund, Germany). Embryos were carefully removed from the amniotic sacs under a dissection microscope and transferred into fresh HBSS. The midbrain (mesencephalon) was dissected out, separated from the diencephalon, and the meninges were meticulously removed. Dissected mesencephalic tissues were then placed into 15 mL Falcon tubes (601,052; Nest, New Jersey, USA) containing HBSS and transferred to a sterile laminar flow hood. The buffer was replaced with 1 mL of 0.05% Trypsin–EDTA (T4049; Sigma, Darmstadt, Germany), pre-warmed to 37 °C, and incubated for 5–10 min to enzymatically dissociate the tissue. Enzymatic activity was halted by adding 1 mL of a trypsin-inactivation solution consisting of 50% fetal bovine serum (FBS) (FBS-16B; Capricorn, Ebsdorfergrund, Germany) in HBSS, followed by a 2-min incubation. After inactivation, the tissues were washed using a complete culture medium composed of Dulbecco's Modified Eagle Medium (DMEM)/Ham's F12 (1:1) with L-glutamine (DMEM-12-A; Capricorn, Ebsdorfergrund, Germany), supplemented with 10% FBS, 1% penicillin–streptomycin (PS-B; Capricorn, Ebsdorfergrund, Germany), 5% bovine serum albumin (BSA) (A9418; Sigma, Darmstadt, Germany), and 1% N2 supplement (N2-K; Capricorn, Ebsdorfergrund, Germany). The tissue was then gently triturated to obtain a single-cell suspension and centrifuged at 400 × g for 5 min. The supernatant was discarded, and the cell pellet was resuspended in 1 mL of complete medium.

To assess cell viability and concentration, 10 µL of the suspension was mixed with 90 µL of Trypan Blue solution (T8154; Sigma, Darmstadt, Germany), and viable cells were counted. The cell concentration was adjusted to 1,500 cells/µL using the complete medium.

Approximately 3×10^5 cells were seeded onto 24-well plates containing Poly-L-Ornithine-coated German coverglasses (GG-12-PLO; Neuvitro, Washington, USA) and incubated at 37 °C for 24 h. After initial attachment, 400 µL of complete medium was added to each well, and the cultures were incubated overnight. On the subsequent day, 500 µL of fresh complete medium was added. Medium changes were performed every other day over a five-day period to facilitate neuronal differentiation.

To verify dopaminergic identity, cells were subjected to immunofluorescence staining using an antibody against tyrosine hydroxylase (TH) (sc-25269; Santa Cruz Biotechnology, Texas, USA) a well-established marker of dopaminergic neurons. Briefly, cells were fixed with 4% paraformaldehyde, permeabilized with 0.1% Triton X-100 (X100; Sigma, Darmstadt, Germany), and incubated overnight at 4 °C with the primary anti-TH antibody (1:200 dilution). After phosphate buffered saline (PBS) (P4417; Sigma, Darmstadt, Germany) washing steps, samples were incubated with a secondary antibody and counterstained with Fluoroshield Mounting Medium with DAPI (F6057; Sigma, Darmstadt, Germany) to visualize cell nuclei [29]. Fluorescence signals were examined under a fluorescent microscope (BX-51; Olympus, Tokyo, Japan), and TH-positive cells were quantified to confirm dopaminergic phenotype.

Preparation of Niosome-siRNA Complexes

Niosomes are vesicular structures composed of non-ionic surfactants, structurally similar to liposomes, and have shown significant promise in improving the systemic delivery and stability of therapeutic molecules, such as siRNA [30, 31]. They are also capable of penetrating the BBB effectively [23]. Considering this evidence, niosomes were selected as the delivery vehicle for siRNA in the current study.

The niosomes were prepared using the thin-film hydration technique as previously described[32]. Briefly, Span 60 (S7010; Sigma, Darmstadt, Germany) and cholesterol (PHR1533; Sigma, Darmstadt, Germany) were combined in equimolar concentrations (20 mM) and dissolved in a chloroform/methanol mixture (2:1 v/v). The organic solvents were evaporated using a rotary evaporator (Buchi R-3, Flawil, Switzerland), forming a uniform lipid film on the flask wall. For the hydration step, siRNAs (1,330,003; Thermo, Waltham, USA) was diluted in PBS and added to the dried lipid layer. The mixture was incubated on a mechanical shaker at 60 °C for 2 h. To reduce the particle size, probe sonication was applied for 30 min. Unencapsulated siRNA was removed by centrifugation at 7,000 rpm for 15 min with a single PBS wash [33]. To prolong systemic circulation time, the niosome-siRNA complexes were PEGylated using DSPE-PEG-2000 (880127P; Sigma, Darmstadt, Germany),

as outlined by Huang et al. [34]. Finally, the PEGylated complexes were lyophilized for long-term storage and subsequent use [35].

Characterization of Niosome-siRNA Complexes

The physicochemical properties of GCN5-targeting siRNA-loaded niosomes were assessed by dynamic light scattering (DLS), which provided measurements for average particle size, zeta potential, and polydispersity index (PDI). The structural morphology of the complexes was further examined using Transmission Electron Microscopy (TEM) to confirm vesicle formation and integrity.

To determine the siRNA encapsulation efficiency, High-Performance Liquid Chromatography (HPLC) analysis was employed. The encapsulation percentage was calculated using the following equation [36]:

$$EE\% = \left[(totalsiRNA - freesiRNA)/totalsiRNA\right] \times 100$$

The in vitro release profile of siRNA from the niosomal formulation was evaluated using the dialysis method. A defined quantity of the complex was loaded into a dialysis membrane with a 12 kDa molecular weight cut-off and placed in 10 mL of PBS (pH 7.4). The system was maintained at 37 °C with gentle stirring (70 rpm) for 12 h. At predetermined intervals, 1 mL aliquots were withdrawn and replaced with fresh buffer of equal volume, pre-warmed to 37 °C.

Quantification of the released siRNA was carried out using UV–Vis spectrophotometry (Perkin Elmer, Waltham, USA), and the release percentage was determined based on a standard calibration curve, referencing the original loading concentration [37].

Selection of Effective siRNA for GCN5 Silencing

To determine the most potent siRNA sequence for silencing the GCN5 gene, previously characterized primary mesencephalic dopaminergic neuron cultures were utilized. Experimental design consisted of four groups, each containing 3×10^5 cells: a control group and three treatment groups exposed to different siRNA constructs, siRNA 1 (RSS314385), siRNA 2 (RSS314386), and siRNA 3 (RSS314387). The control group received only niosomes without siRNA, while each treatment group was administered 100 nM of the respective siRNA encapsulated within niosomes, added directly to the culture medium [38].

All cultures were maintained at 37 °C for 48 h under standard conditions. Each experiment was conducted in triplicate to ensure reproducibility.

After incubation, cells were harvested through trypsinization and prepared for subsequent analyses to evaluate the gene silencing efficacy of each siRNA sequence. For gene expression analysis, total RNA was extracted, reverse-transcribed into cDNA, and subjected to real-time quantitative PCR (RT-qPCR) using specific primers listed in Table 2. Relative gene expression levels were calculated using the $2^{\wedge -\Delta\Delta Ct}$ method, normalized to GAPDH expression [39]. In parallel, cells were assessed at the protein level using immunofluorescence staining [29] with anti-GCN5 primary antibody (sc-365321; Santa Cruz Biotechnology, Texas, USA) diluted 1:200, allowing visualization of residual protein expression following siRNA transfection.

In Vivo Experimental Design

In total, 96 adult male SD rats (190–220 g) were utilized for the in vivo phase of the study. Animals were sourced from the Ege University Laboratory Animals Research and Application Center (Izmir, Turkey). They were housed in standard polypropylene cages under controlled environmental conditions (22 ± 2 °C temperature, 50 ± 10% relative humidity, 12-h light/dark cycle) with unrestricted access to standard pellet feed and water.

All experimental protocols complied with the ARRIVE 2.0 guidelines [40].

Rats were randomly assigned to four groups (n = 24 per group), as outlined below:

- **Control Group (n = 24):** No pharmacological or surgical intervention was performed. Animals were subjected to daily handling identical to experimental groups to reduce stress-related confounding. All animals were sacrificed on Day 42.
- **Rotenone (ROT) Group (n = 24):** A subacute model of PD was induced via subcutaneous administration of rotenone at a dose of 2 mg/kg/day for 35 consecutive days (5 weeks) [41]. Two hours after the final subcutaneous rotenone dose, the animals received three intravenous injections of physiological saline via the lateral tail vein at 48-h intervals,.No additional treatment was provided. Sacrifice was carried out on Day 42.
- **ROT + Empty Niosome Group (n = 24):** PD model induction followed the same rotenone protocol. Two hours after the final subcutaneous rotenone administration, 150 µg of empty niosomes suspended in physiological saline were injected intravenously via the tail vein at 48-h intervals, for a total of three administrations [38]. Animals were sacrificed on Day 42.
- **ROT + GCN5 siRNA Group (n = 24):** Two hours after the PD model induction with subcutaneous administration of rotenone, animals received 150 µg of GCN5-targeted niosome-siRNA complex in physiological saline, delivered intravenously via the tail vein. The injection schedule mirrored the previous group, with three total

doses administered every 48 h starting 2 h post-final rotenone injection [38]. All animals were sacrificed on Day 42.

Rotenone (R8875; Sigma, Darmstadt, Germany) was freshly prepared before each use by dissolving it in a 1:9 mixture of dimethyl sulfoxide (DMSO) (sc-358801; Santa Cruz Biotechnology, Texas, USA) and sunflower oil, with preparation conducted in the dark to maintain chemical stability. Intravenous administrations were carried out aseptically through the lateral tail vein.

Behavioral Tests

To assess motor behavior and Parkinsonian-like symptoms, the Open Field Test (OFT) and Catalepsy Bar Test (CBT) were employed, respectively, on randomly selected subsets of eight rats per group on days 0, 21, and 42 [42, 43].

The OFT was conducted in a square arena measuring 72 cm × 72 cm, divided into 16 equal squares and enclosed by 36-cm-high opaque walls. Each rat was placed in the center of the arena, and its spontaneous activity was monitored and recorded over a 5-min session. Between trials, the apparatus was cleaned with 70% ethanol to prevent olfactory cues. Behavioral parameters assessed included immobility time, rearing frequency, number of squares crossed (indicative of locomotor activity), and total horizontal distance traveled [42].

For the CBT, rats were gently placed in a semi-upright posture with their forepaws positioned on a horizontal bar elevated 9 cm above the surface. A stopwatch was initiated immediately upon positioning, and the latency to withdraw at least one paw and make contact with the ground was measured. Trials were terminated if the animal failed to respond within 180 s [43].

In Vivo Imaging System (IVIS) Analysis

IVIS technology facilitates non-invasive visualization of the biodistribution of administered agents by detecting fluorescence or bioluminescence signals in small animal models [44]. In the current study, IVIS analysis was performed on a cohort of eight rats from the ROT + GCN5 siRNA group, which were also subjected to behavioral assessments. The Niosome-siRNA complexes were fluorescently labeled with Cyanine5 (Cy5) (M046080; Sigma, Darmstadt, Germany), and imaging was conducted using the IVIS Spectrum System (Perkin Elmer, Waltham, USA). Excitation and emission filters were set to 615–665 nm and 695–770 nm, respectively. Whole-body fluorescent images were acquired at multiple time points post-injection (1, 3, 5, 24, 48, and 72 h) to evaluate the temporal and spatial distribution of the complexes throughout the organism.

Assessment of Oxidative Stress and Neurochemical Markers

Eight rats from each experimental group were randomly selected and euthanized under anesthesia via cervical dislocation, followed by decapitation. Brains were rapidly removed, and midbrain regions were dissected on ice with reference to Paxinos and Watson's rat brain atlas [45]. The isolated midbrain tissues were homogenized and homogenates were centrifuged at 14,000 × g for 20 min at 4 °C, and the resulting supernatants were collected and stored at − 80 °C for subsequent biochemical analysis via enzyme-linked immunosorbent assay (ELISA).

To evaluate lipid peroxidation, tissues were homogenized using MDA Lysis Buffer and centrifuged at 13,000 × g for 10 min according to the manufacturer's instructions. Malondialdehyde (MDA) levels were quantified using a commercial MDA ELISA Kit (E-EL-0060; Elabscience, Houston, TX, USA). Absorbance was measured at 532 nm using a microplate reader (Multiskan TM FC; Thermo, Waltham, USA).

For assessment of antioxidant capacity, superoxide dismutase (SOD) activity was determined using a Superoxide Dismutase Activity Assay Kit (E-EL-R1424; Elabscience), following the manufacturer's protocol. Tissues were homogenized in ice-cold Tris–HCl buffer (pH 7.4) containing Triton X-100, β-mercaptoethanol (β-ME), and phenylmethylsulfonyl fluoride (PMSF). After centrifugation at 14,000 × g for 5 min at 4 °C, the supernatants were collected and analyzed spectrophotometrically at 450 nm.

Dopamine (DA) concentrations were quantified using a rat-specific Rat Dopamine (DA) ELISA Kit (MBS262606; Mybiosource, San Diego, USA). All assays were performed in accordance with the manufacturers' protocols, and absorbance was recorded at 450 nm using a microplate reader.

Tissue Processing and Histological Staining

Eight animals from each experimental group were euthanized via intracardiac perfusion with 4% paraformaldehyde (PFA) (158,127; Sigma, Darmstadt, Germany). Brains were harvested, post-fixed in 4% PFA for 48 h, and midbrain regions were dissected in accordance with rat brain atlas [45]. Tissues were processed through a graded ethanol series for dehydration, cleared in xylene, and embedded in paraffin. Coronal Sects. (5 µm thickness) were serially cut for histological and immunohistochemical evaluations.

To evaluate general cytoarchitecture, sections were deparaffinized, rehydrated, and stained with hematoxylin for 3 min. Following differentiation in acid alcohol and bluing in ammoniated water, eosin staining was applied for 1 min. Sections were dehydrated, cleared, and mounted using Entellan (1.07960; Sigma, Darmstadt, Germany).

Table 1 The primer antibodies used in IHC analysis

Antibody	Catalog No/Manufacturer	Dilution ratio
GCN5	sc-25269/Santa Cruz Biotechnology, Texas, USA	1:100
Parkin	sc-32282/Santa Cruz Biotechnology, Texas, USA	1:50
Pink1	sc-517353/Santa Cruz Biotechnology, Texas, USA	1:50
Mfn2	sc-100560/Santa Cruz Biotechnology, Texas, USA	1:100
Phospho-Drp1 (Ser616)	bs-12702R/Bioss, Massachusetts, USA	1:200
PGC-1α	bs-7535R/Bioss, Massachusetts, USA	
TH	sc-365321/Santa Cruz Biotechnology, Texas, USA	1:100
Phospho-α-syn (Ser129)	ab51253/Abcam, Cambridge, UK	1:500

Toluidine blue (T3260; Sigma, Darmstadt, Germany) staining was performed to further assess the morphology of dopaminergic neurons in the midbrain. After deparaffinization and rehydration, sections were incubated in 1% toluidine blue solution (pH 4.4) for 2–3 min, rinsed in distilled water, dehydrated through ascending alcohols, cleared in xylene, and coverslipped.

Immunohistochemical Analysis, Image Acquisition and Quantitative Analysis

To block endogenous peroxidase activity, sections were treated with 10% hydrogen peroxide (H_2O_2) (H1009; Sigma, Darmstadt, Germany) for 30 min, followed by a 1-h incubation in blocking buffer (SHP125; Scytec, Utah, USA) at room temperature. Sections were then incubated overnight at 4 °C with primary antibodies (Table 1). After rinsing, biotinylated secondary antibodies and horseradish peroxidase (HRP)-conjugated streptavidin (SHP125; Scytec, Utah, USA) were applied. Immunoreactivity was visualized using 3,3′-diaminobenzidine (DAB) (ACK125; Scytec, Utah, USA) substrate and counterstained with Mayer's Hematoxylin (MHS32; Sigma, Darmstadt, Germany).

Images were acquired using a light microscope (BX5; Olympus, Tokyo, Japan). For each animal, three randomly selected coronal sections were analyzed, each comprising ten non-overlapping fields within the ventral midbrain. Immunopositive areas were quantified using ImageJ software (Version 1.46; National Institutes of Health, Maryland, USA). Color thresholding was applied to isolate stained regions, which were then expressed as a percentage of the total tissue area. Integrated density values were normalized, and data were represented as the ratio of immunopositive to total tissue area [46].

RT-qPCR Analysis

Midbrain tissues (n = 4) and primary mesencephalic dopaminergic neuron cultures were homogenized in 1 mL of TriPure Isolation Reagent containing guanidinium thiocyanate (11,667,165,001; Roche Applied Science, Penzberg, Germany) using a glass-Teflon homogenizer. Total RNA was isolated according to the manufacturer's instructions provided with the TriPure reagent. RNA quality and quantity were assessed spectrophotometrically. For

Table 2 The forward and reverse primers employed for qRT-qPCR analysis

Gene	Primer sequences	Referance
GCN5	Forward: 5'-CATCGGTGGGATTTGCTT-3' Reverse: 5'-GTACTCGTCGGCGTAGGTG-3'	[48]
Parkin	Forward: 5′-CCGAGTGACACTGATAGTGTTTGT-3 Reverse: 5′-ATCGTCTGCGGATTGGCTGTAGTT-3′	[49]
Pink1	Forward: 5′-CATGGCTTTGGATGGAGAGT-3′ Reverse: 5′-TGGGAGTTTGCTCTTCAA GG-3′	[50]
Mfn2	Forward: 5′-CTGCCAACCCCAGCATGCCA-3′ Reverse: 5′-GGCGCTTGAAGGCCCTCTCC-3′	[50]
Drp1	Forward: 5′-ACTGGCCCCCGTCCAGCTTA-3′ Reverse: 5′-TGAT CCACATCTGCTGGAAGGT-3′	[50]
PGC-1α	Forward: 5′-CCGAGAATTCATGGAGCAAT-3′ Reverse: 5'-GTGTGAGGAGGGTCATCGTT-3'	[51]
GAPDH (Referans Gene)	Forward: 5'- GGATGCAGGGATGATGTTCT −3' Reverse: 5'- AAGGGCTCATGACCACAGTC −3'	[52]

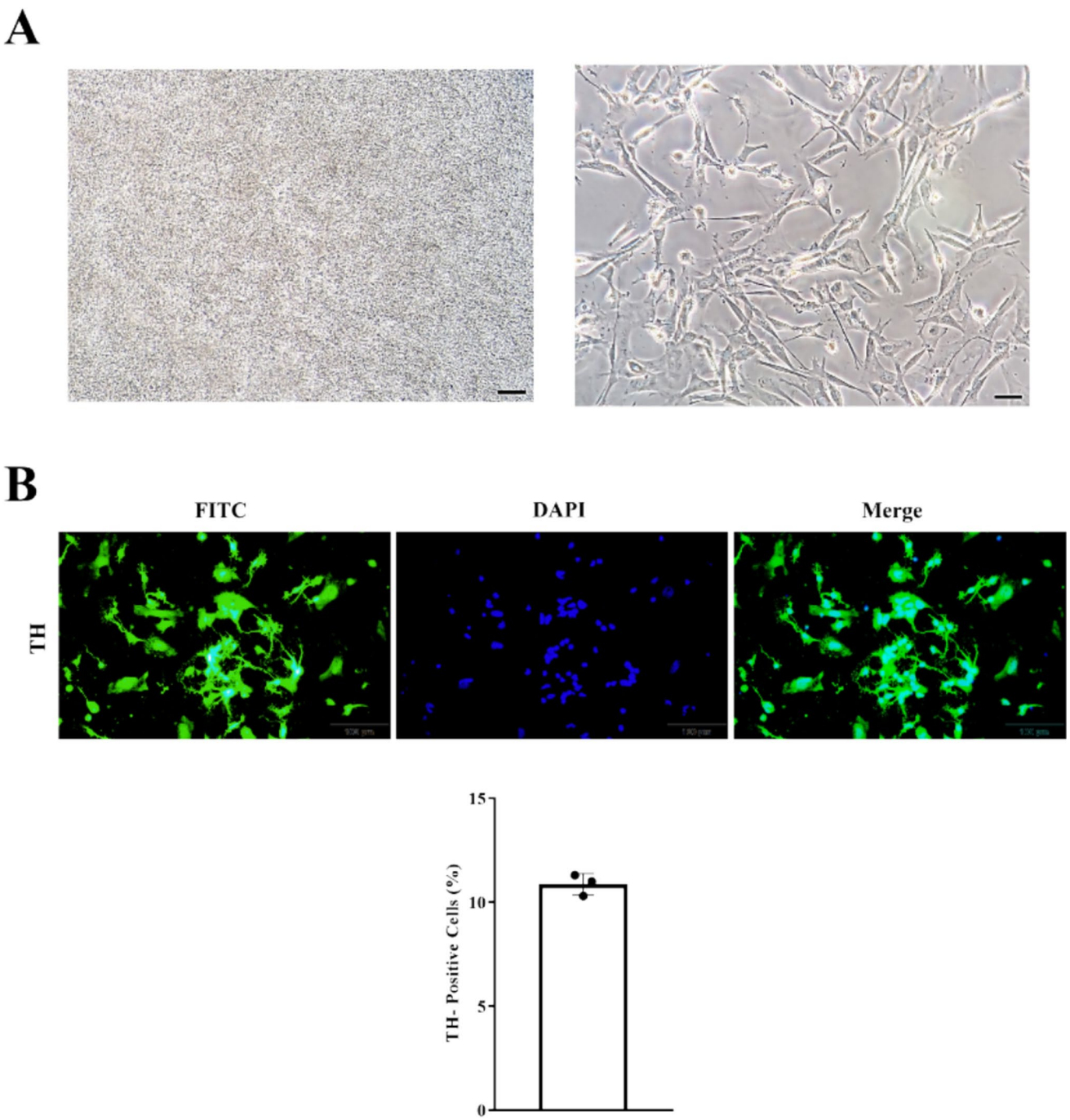

Fig. 1 Images depicting the morphological development of cultured primary midbrain dopaminergic neurons at day 0 (left panel) and day 7 (right panel) (**A**), showing the shift from an initially round appearance to a mature neuronal morphology (scale bar: 50 µm). Immunocytochemical staining for tyrosine hydroxylase (TH) was performed to identify dopaminergic neurons in the culture (**B**). TH-positive cells following immunocytochemical staining (scale bar: 100 µm). TH-positive neurons were expressed as a percentage of total DAPI-positive cells based on counts of 300 cells per evaluation. Counting process was independently performed by three histologists. Data are presented as mean ± SD. Individual data points represent independent evaluations

cDNA synthesis, 1 µg of total RNA from each sample was reverse-transcribed using the Transcriptor First Strand cDNA Synthesis Kit (11,483,188,001; Roche, Darmstadt, Germany), following the supplied protocol.

RT-qPCR was performed using SYBR® Green PCR Master Mix (4,364,346; Thermo, Waltham, USA) on a LightCycler 480 Real-Time PCR System (Roche, Darmstadt, Germany). GAPDH was used as the endogenous

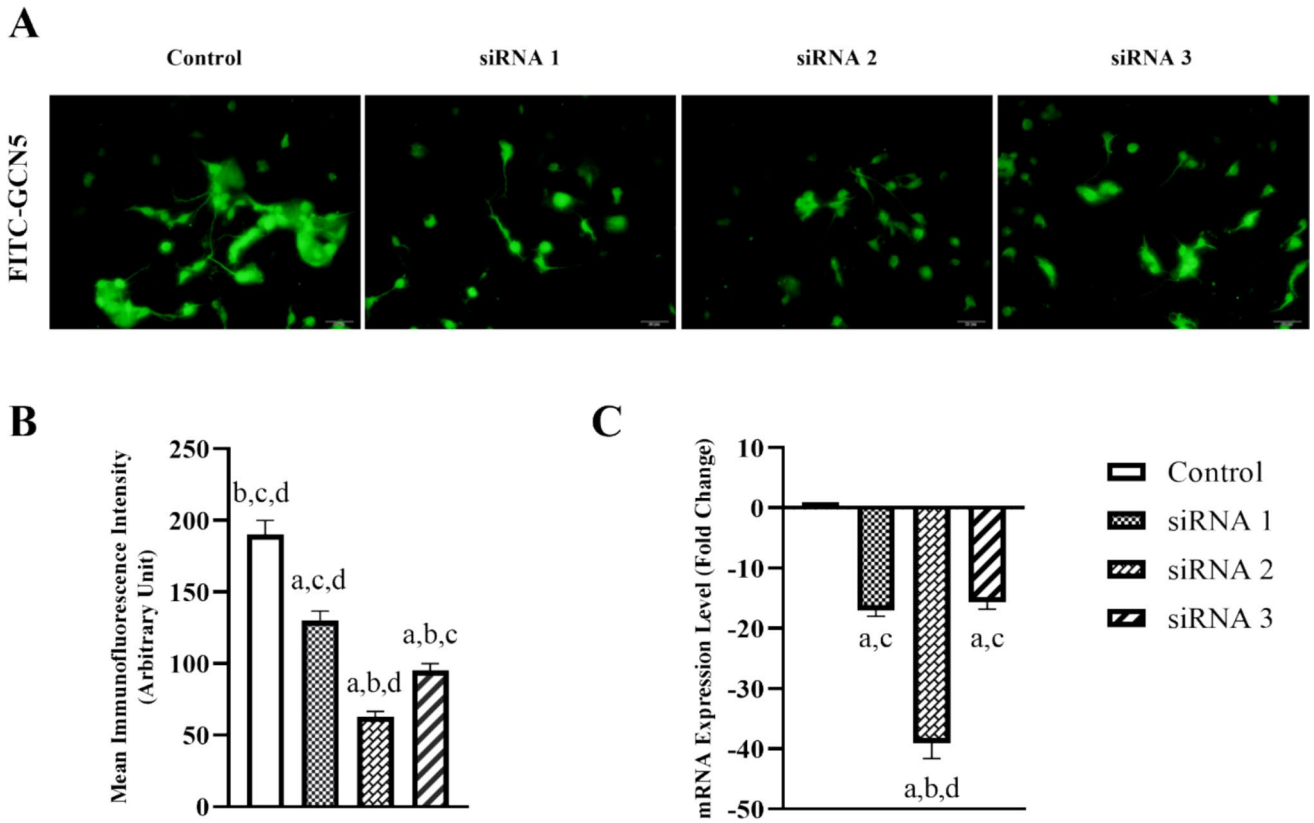

Fig. 2 Immunofluorescence staining of GCN5 in cultured primary midbrain dopaminergic neurons from the Control, siRNA 1 (RSS314385), siRNA 2 (RSS314386), and siRNA 3 (RSS314387) treatment groups (scale bar: 20 µm) (A), along with the corresponding quantification of mean fluorescence intensity (B). Relative mRNA expression levels of GCN5, determined by RT-qPCR, in the same experimental groups (C). Results indicate that siRNA 2 induces the most pronounced downregulation of GCN5 at both the immunoreactivity and transcript levels. a: significant change compared to the Control Group ($p < 0.05$), b: significant change compared to the siRNA 1 ($p < 0.05$), c: significant change compared to the siRNA 2 ($p < 0.05$), d: significant change compared to the siRNA 3 ($p < 0.05$) Data represent mean ± SD of n = 3 independent experiments, each performed in triplicate

control gene, and all reactions were run in triplicate. Relative mRNA expression levels were calculated using the $2^{-(\Delta\Delta Ct)}$ method [47].

The primer sequences used in this study are listed in Table 2.

Statistical Analysis

We utilized GraphPad Prism 5 software (GraphPad Software, Inc., La Jolla, CA) for statistical analysis. Following completion of all experiments, group comparisons were assessed using one-way analysis of variance (ANOVA) followed by post-hoc Tukey tests. Data were presented as mean ± standard error, with statistical significance set at $p < 0.05$, $p < 0.001$, and $p < 0.0001$.

Results

Phenotypic and Molecular Features of Primary Midbrain Dopaminergic Neurons

Primary mesencephalic dopaminergic neuronal cultures were established using embryos (n = 16) harvested at embryonic day 14.5 (E14.5) from two timed-pregnant rats. Following enzymatic dissociation, cell viability and total yield were assessed via Trypan Blue staining and this assay revealed a total yield of approximately 19.2×10^6 cells, with a viability rate of 93.01%.

At 24 h post-seeding, cells predominantly exhibited a rounded morphology; however, by day 7 in vitro, they had adopted neuron-specific morphological features (Fig. 1).

To quantify the dopaminergic neuron subpopulation within the culture, immunocytochemical labeling was

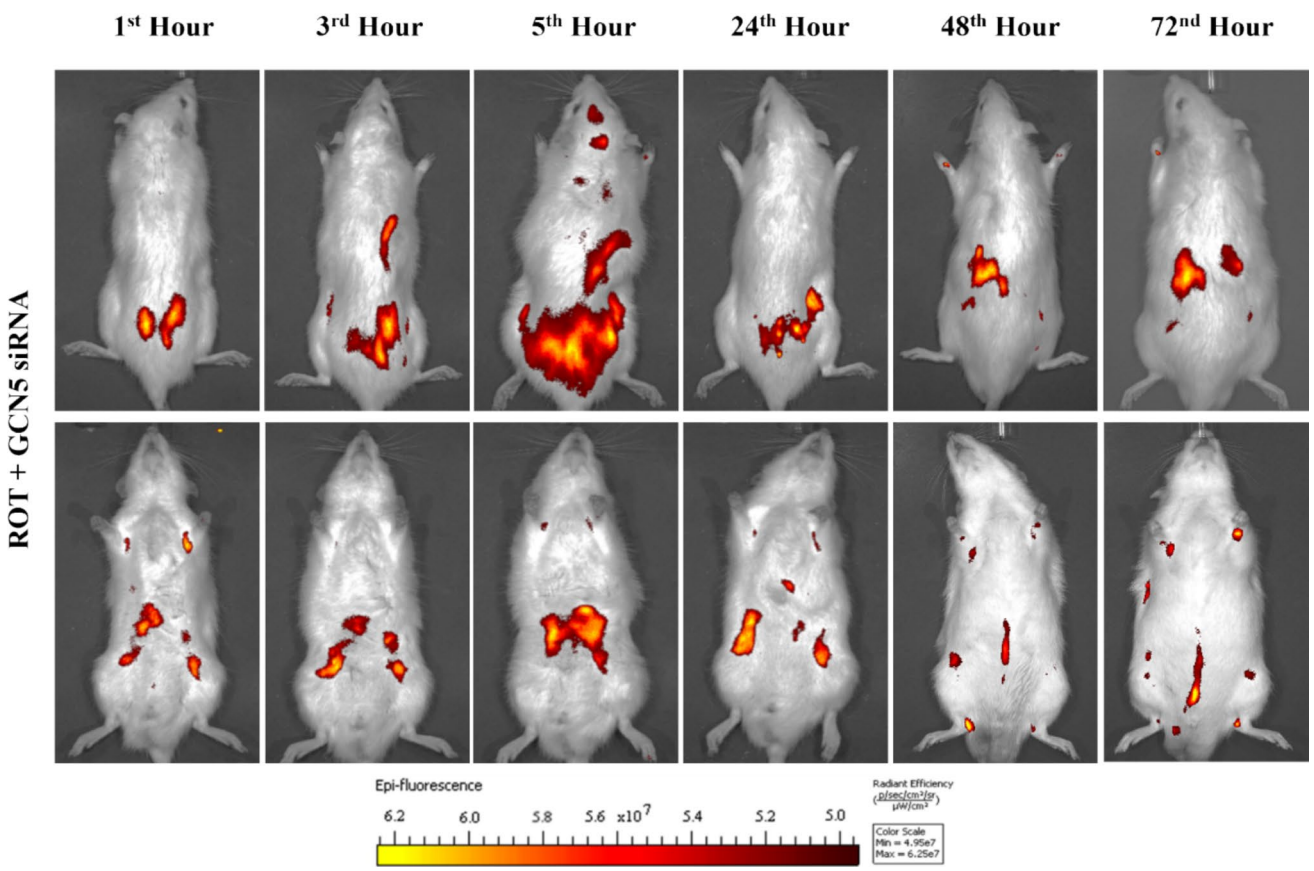

Fig. 3 Time-dependent biodistribution of the niosome–siRNA complex visualized via IVIS imaging. Strong fluorescence signals were detected in the brain within 3 to 5 h following systemic administration, indicating successful central accumulation. Signal intensity progressively declined over 24 h, with predominant localization shifting to the renal and bladder regions by 48 and 72 h, suggesting renal clearance as the main elimination route. The persistence of detectable signal beyond 72 h reflects extended systemic circulation

carried out using tyrosine hydroxylase (TH) as a dopaminergic marker (Fig. 1). Analysis indicated that TH-positive neurons comprised roughly 10–11% of the total cell population, in agreement with established values in the literatüre [53].

Findings on Characterization of Niosome and Niosome–siRNA Complex

DLS analysis demonstrated that the average hydrodynamic diameter of the blank niosomes was 283.3 ± 0.65 nm, accompanied by a zeta potential of -23.3 ± 0.31 mV and a polydispersity index (PDI) of 0.316 ± 0.025. In contrast, niosomes complexed with siRNA exhibited an average size of 335.7 ± 0.73 nm, a zeta potential of -23.6 ± 0.25 mV, and a PDI of 0.354 ± 0.023 (Figure S1).

Transmission Electron Microscopy (TEM) was employed to further characterize both unloaded and siRNA-loaded vesicles. TEM micrographs revealed that both formulations retained a spherical morphology. The particle size observed via TEM ranged between 90–100 nm, notably smaller than the DLS measurements, which is attributable to the fact that DLS assesses the hydrodynamic diameter, including the solvation layer surrounding the nanoparticles (Figure S1).

High-performance liquid chromatography (HPLC) analysis indicated an siRNA encapsulation efficiency of 45%, corresponding to approximately 7.2 nmol of siRNA entrapped per 16 nmol initially introduced into the formulation process.

Release kinetics studies revealed a biphasic release pattern: nearly 41% of the encapsulated siRNA was discharged within the first 3 h, indicative of an initial burst phase, followed by a sustained release extending up to 12 h. By the end of the observation period, close to 90% of the siRNA payload had been released (Figure S1). This biphasic release profile is considered advantageous, as the early surge may enhance penetration across the blood–brain barrier via transient concentration gradients, while the subsequent sustained phase ensures prolonged therapeutic delivery.

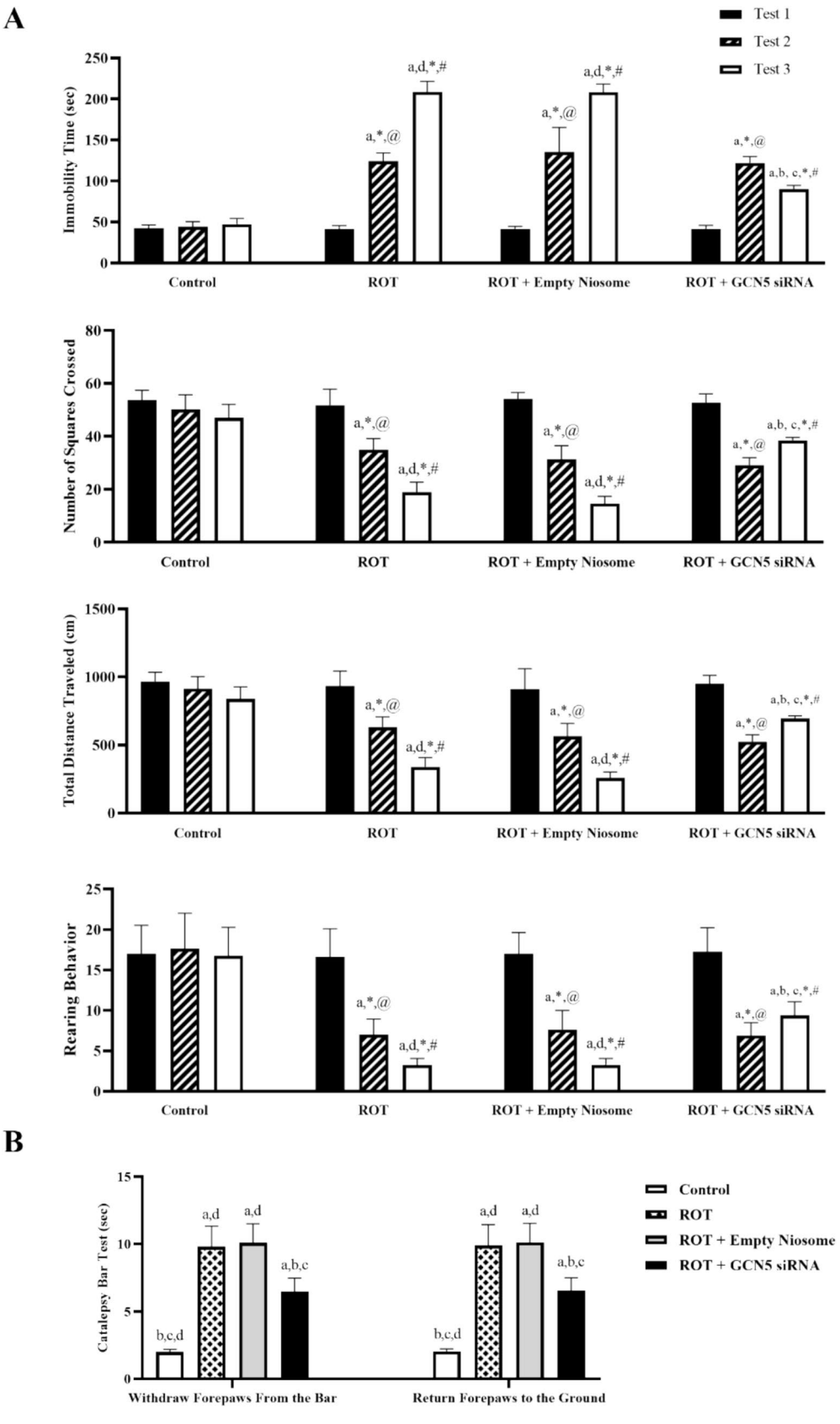
A
Test 1
Test 2
Test 3
Immobility Time (sec)
Number of Squares Crossed
Total Distance Traveled (cm)
Rearing Behavior
Control
ROT
ROT + Empty Niosome
ROT + GCN5 siRNA
B
Catalepsy Bar Test (sec)
Withdraw Forepaws From the Bar
Return Forepaws to the Ground
Control
ROT
ROT + Empty Niosome
ROT + GCN5 siRNA

◂**Fig. 4** Behavioral performance assessed by the Open Field Test (A) and Catalepsy Bar Test (B). At baseline (day 0), all groups exhibited comparable locomotor activity. By days 21 and 42, animals in the ROT, ROT + Empty Niosome, and ROT + GCN5–siRNA groups displayed increased immobility relative to the Control group. However, the ROT + GCN5–siRNA group showed significant functional improvement compared to the untreated Parkinsonian groups. Catalepsy assessment on day 42 revealed elevated scores in all rotenone-treated groups, whereas siRNA-treated animals demonstrated a substantial reduction in cataleptic response, indicating partial restoration of motor function. a: Significant difference compared to the Control group ($p < 0.0001$). b: Significant difference compared to the ROT group ($p < 0.0001$). c: Significant difference compared to the ROT + Empty Niosome group ($p < 0.0001$). d: Significant difference compared to the ROT + GCN5–siRNA group ($p < 0.0001$). *: Significant difference compared to the first behavioral test ($p < 0.0001$). #: Significant difference compared to the second behavioral test ($p < 0.0001$). @: Significant difference compared to the third behavioral test ($p < 0.0001$)

Results on Selection of Effective siRNA for GCN5 Silencing

qRT-PCR analysis revealed a marked downregulation of GCN5 mRNA expression following a 48-h incubation with siRNA 2 (RSS314386), showing an approximate 39.12-fold decrease relative to untreated control cells. Furthermore, GCN5 transcript levels in the siRNA 2-treated group were 2.29-fold and 2.49-fold lower than those observed in the siRNA 1 (RSS314385) and siRNA 3 (RSS314387) groups, respectively (Fig. 2).

Corroborating the transcript-level findings, immunofluorescence (IF) staining demonstrated a pronounced reduction in GCN5 protein expression in the siRNA 2-treated condition compared to all other experimental groups (Fig. 2).

Taken together, these data indicate that siRNA 2 (RSS314386) exerts the most potent inhibitory effect on GCN5 expression at both transcriptional and translational levels. Consequently, this siRNA was selected for subsequent in vivo investigations.

Niosomal Transport Facilitates Brain Delivery of GCN5-Specific siRNAs

In vivo fluorescence imaging via IVIS revealed that the niosome–siRNA complex localized to the brain within 3 to 5 h following systemic administration (Fig. 3). A progressive decline in cerebral fluorescence intensity was observed over the subsequent 24 h, suggesting efficient clearance from neural tissues. By 48 and 72 h post-injection, fluorescence signals were predominantly concentrated in the renal and bladder regions, indicating that renal excretion may serve as the principal elimination route. These results imply that the niosome–siRNA complex exhibits a prolonged circulation time, with a biological half-life exceeding 72 h.

GCN5 Silencing Enhances Motor Functional Recovery

In the initial OFT performed on day 0 (Test 1), no statistically significant differences were observed among experimental groups regarding immobility duration, number of squares traversed, total distance covered, or rearing activity (Fig. 4A). By day 21 (Test 2), animals in the ROT, ROT + Empty Niosome, and ROT + GCN5 siRNA groups exhibited a marked increase in immobility time alongside a significant reduction in locomotor parameters—including the number of squares crossed, total movement distance, and rearing frequency—when compared to the Control group. These motor deficits persisted through day 42 (Test 3), with all three Parkinson-model groups again showing significantly impaired performance relative to controls across the same parameters. Notably, animals in the ROT + GCN5 siRNA group displayed a significant amelioration in motor function compared to both the ROT and ROT + Empty Niosome groups, as evidenced by reduced immobility time and improved measures of ambulation and exploratory behavior.

On day 42, the concluding day of the study, the catalepsy bar test (CBT) was administered in triplicate per animal to assess motor rigidity. Two metrics were evaluated: the latency to remove the forepaws from the horizontal bar and the time to return the forepaws to the ground. Statistical analysis indicated that the ROT, ROT + Empty Niosome, and ROT + GCN5 siRNA groups all demonstrated elevated catalepsy scores relative to the Control group (Fig. 4B). However, the ROT + GCN5 siRNA group exhibited a significant reduction in cataleptic response compared to the other Parkinsonian groups, suggesting partial restoration of motor function.

GCN5 Silencing Alleviates Oxidative Stress and Histopathological Alteration in a Rotenone-Induced Parkinson's Disease Model

Silencing of the GCN5 gene significantly attenuated both oxidative stress markers and neuropathological alterations in rats subjected to rotenone (Fig. 5).

A marked increase in MDA levels was observed across all rotenone-exposed groups compared to the Control group, reflecting elevated oxidative damage. However, MDA concentrations were significantly reduced in the ROT + GCN5 siRNA group relative to both the ROT and ROT + Empty Niosome groups (Fig. 5A). Furthermore, rotenone exposure caused a significant decline in SOD activity, indicative of impaired antioxidant defense. Notably, GCN5 gene silencing led to a significant restoration of SOD levels, with the ROT + GCN5 siRNA group exhibiting higher SOD activity than other rotenone-treated cohorts (Fig. 5A).

Histopathological examination of midbrain sections stained with HE and TB revealed severe dopaminergic neurodegeneration in the SNpc of rotenone-treated rats. Typical neuropathological hallmarks included reactive gliosis, pyknosis, cytoplasmic inclusions resembling Lewy bodies, and neuronal swelling. In contrast, rats treated with GCN5 siRNA exhibited substantially preserved tissue integrity, with midbrain architecture and cellular morphology closely resembling that of the Control group (Fig. 5B).

These findings collectively suggest that GCN5 silencing confers neuroprotection by reducing oxidative stress and mitigating Parkinsonism-associated histological damage.

GCN5 Knockdown Confers Neuroprotection Against Parkinsonism-Related Pathology via Regulation of Mitochondrial Dynamics-Associated Genes

IHC and RT-qPCR analyses demonstrated that the GCN5 gene was efficiently silenced following administration of the niosome–siRNA complex (Fig. 6). IHC staining revealed a marked upregulation of GCN5 immunoreactivity in PD model groups compared to the Control group. In contrast, animals treated with GCN5-targeting siRNA exhibited a substantial reduction in both the number of GCN5-positive cells and the staining intensity, when compared to the ROT and ROT + Empty Niosome groups. These immunoreactivity -level alterations were further validated by ELISA, which supported the observed downregulation. In parallel, RT-qPCR results showed that GCN5 mRNA expression was decreased by approximately 245.28-fold relative to the ROT group and by 193.80-fold compared to the ROT + Niosome group (Fig. 6A). In contrast to GCN5 expression, IHC analysis of PGC-1α revealed a significant reduction in the number of PGC-1α–positive cells and immunoreactivity in both the ROT and ROT + Empty Niosome groups compared to the Control group (Fig. 6B). However, in the ROT + GCN5 siRNA group, there was a marked increase in both the density of PGC-1α–positive cells and the intensity of immunoreactivity relative to the other rotenone-exposed groups. Complementary RT-qPCR analysis supported these findings, showing that PGC-1α mRNA expression was upregulated by approximately 25.54-fold compared to the ROT group and 20.28-fold relative to the ROT + Empty Niosome group (Fig. 6C).

Immunohistochemical evaluation of Drp-1 revealed a significant increase in the number of Drp-1–positive cells and the intensity of immunoreactivity in both the ROT and ROT + Empty Niosome groups compared to the Control group (Fig. 7A). In contrast, the ROT + GCN5 siRNA group showed a notable reduction in both Drp-1–positive cell count and immunoreactivity relative to the Control group (Fig. 7B). These observations were corroborated by RT-qPCR analysis, which demonstrated that Drp-1 mRNA expression was downregulated by approximately 141.97-fold when compared to the ROT group and by 37.24-fold relative to the ROT + Empty Niosome group (Fig. 7C). Analysis of Mfn2 expression revealed that baseline expression levels were present in the Control group (7A). In the ROT group, a marked reduction was observed in both the number of Mfn2-positive cells and the intensity of Mfn2 immunoreactivity compared to the Control group. In contrast, evaluation of the ROT + Empty Niosome and ROT + GCN5 siRNA groups showed similar numbers of Mfn2-positive cells and comparable immunoreactivity levels, both of which were significantly elevated compared to those in the ROT and Control groups (7B). These findings were further supported by RT-qPCR analysis, which showed that Mfn2 mRNA expression was upregulated by approximately 1.63-fold compared to the ROT group and by 4.07-fold relative to the ROT + Empty Niosome group (Fig. 7C).

Immunohistochemical evaluation of Parkin revealed a significant decrease in the number of Parkin-positive cells and the intensity of immunoreactivity in both the ROT and ROT + Empty Niosome groups compared to the Control group (Fig. 8A). In contrast, the ROT + GCN5 siRNA group exhibited a substantial increase in Parkin immunoreactivity and the number of positive cells, reaching levels comparable to those of the Control group and significantly higher than the other Parkinsonian groups (Fig. 8B). These findings were further corroborated by RT-qPCR analysis, which showed that Parkin mRNA expression was upregulated by approximately 11.36-fold relative to the ROT group and by 21.81-fold compared to the ROT + Empty Niosome group (Fig. 8C). Analysis of Pink1 demonstrated a significant reduction in the number of Pink1-positive cells and immunoreactivity in the ROT and ROT + Empty Niosome groups compared to the Control group (Fig. 8A). In contrast, the ROT + GCN5 siRNA group exhibited a notable increase in both Pink1-positive cell count and immunoreactivity relative to the Control group (Fig. 8B). These results were further supported by RT-qPCR analysis, which showed that Pink1 mRNA expression was elevated by approximately 49.38-fold compared to the ROT group and by 98.81-fold relative to the ROT + Empty Niosome group (Fig. 8C).

Immunohistochemical analysis of tyrosine TH demonstrated a significant reduction in the number of TH-positive neurons and staining intensity across all rotenone-exposed groups (ROT, ROT + Empty Niosome, and ROT + GCN5 siRNA) compared to the Control group (Fig. 9A). However, among the rotenone-treated cohorts, the ROT + GCN5 siRNA group exhibited a notable increase in both the number of TH-positive cells and the intensity of immunoreactivity relative to the other two groups. Moreover, the TH staining pattern in this group most closely resembled that of the Control group, suggesting partial preservation of dopaminergic neuronal integrity (Fig. 9B). Regarding α-syn immunostaining, basal expression levels were observed in

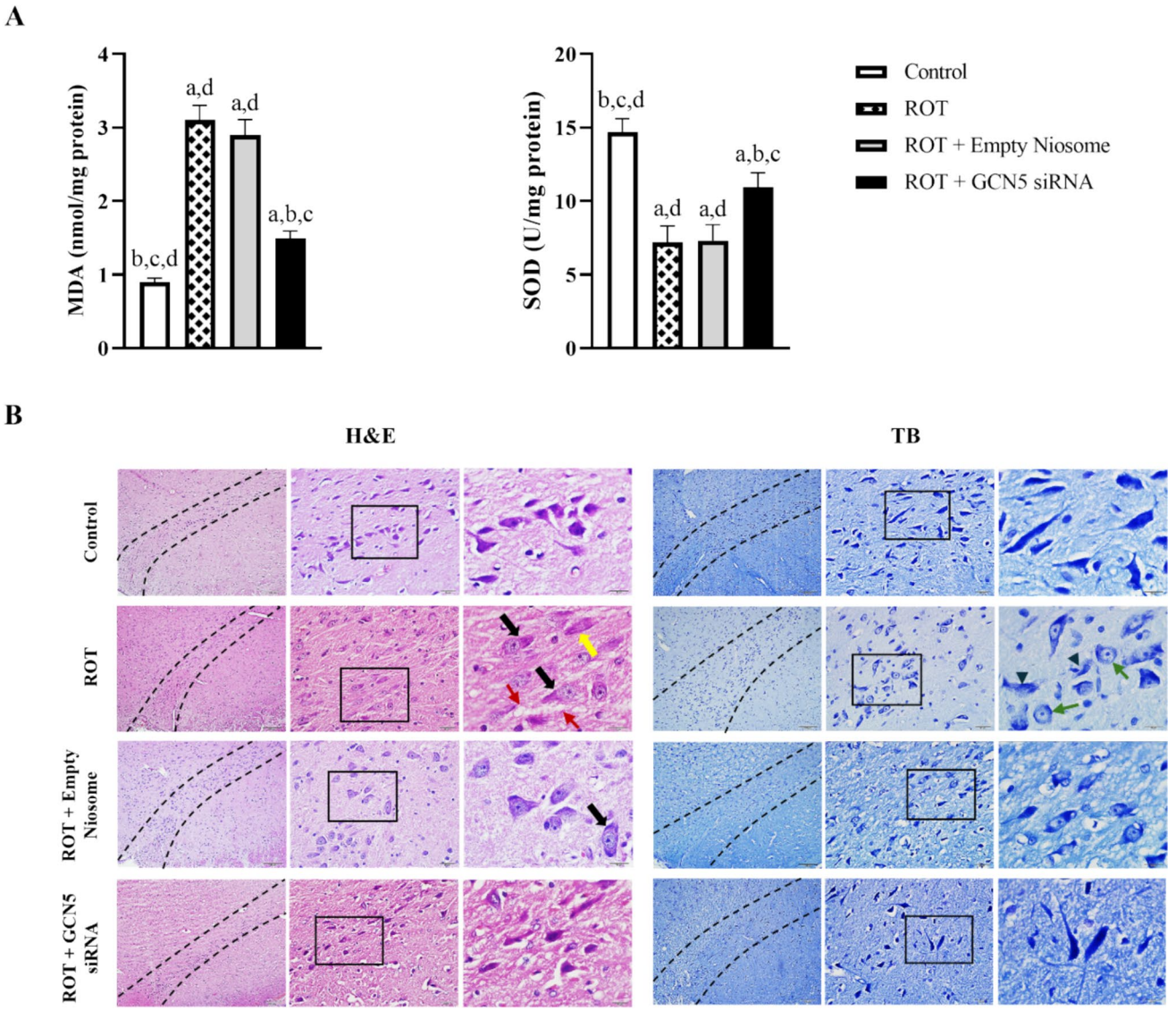

Fig. 5 Evaluation of oxidative stress parameters across experimental groups (**A**). Rotenone exposure significantly reduced SOD activity and increased MDA levels, indicating oxidative damage. GCN5 siRNA treatment restored redox balance, with higher SOD activity and lower MDA levels than both the ROT and ROT + Empty Niosome groups. Histological analysis of the SNpc (**B**). Rotenone induced marked neurodegeneration, including neuronal loss, gliosis, cytoplasmic swelling, and Lewy body-like inclusions. GCN5 silencing preserved SNpc architecture, showing minimal pathology comparable to Control. **Arrows:** black – Lewy body-like inclusions; yellow – Rosenthal fibers; red – vacuolation; green – perikaryal swelling; **Arrow head**– membrane-compromised neurons. a: Significant difference compared to the Control group ($p < 0.0001$). b: Significant difference compared to the ROT group ($p < 0.0001$). c: Significant difference compared to the ROT + Empty Niosome group ($p < 0.0001$). d: Significant difference compared to the ROT + GCN5–siRNA group ($p < 0.0001$)

the Control group. In contrast, a marked upregulation of α-syn expression was detected in all groups subjected to rotenone administration. Notably, among these groups, the ROT + GCN5 siRNA group showed a significant decrease in the number of α-syn–positive cells and immunoreactivity intensity compared to ROT and ROT + Empty Niosome groups (Fig. 9B). Additionally, the α-syn staining profile in this group appeared most similar to that of the Control group, indicating a potential reduction in pathological α-syn accumulation (Fig. 9A). Furthermore, analysis using the dopamine ELISA assay revealed a marked decrease in dopamine levels in all groups exposed to rotenone when compared to the Control group. Notably, within the rotenone-treated groups, the ROT + Niosome–siRNA cohort displayed a significant elevation in dopamine concentrations relative to both the ROT and ROT + Empty Niosome groups (Fig. 9C).

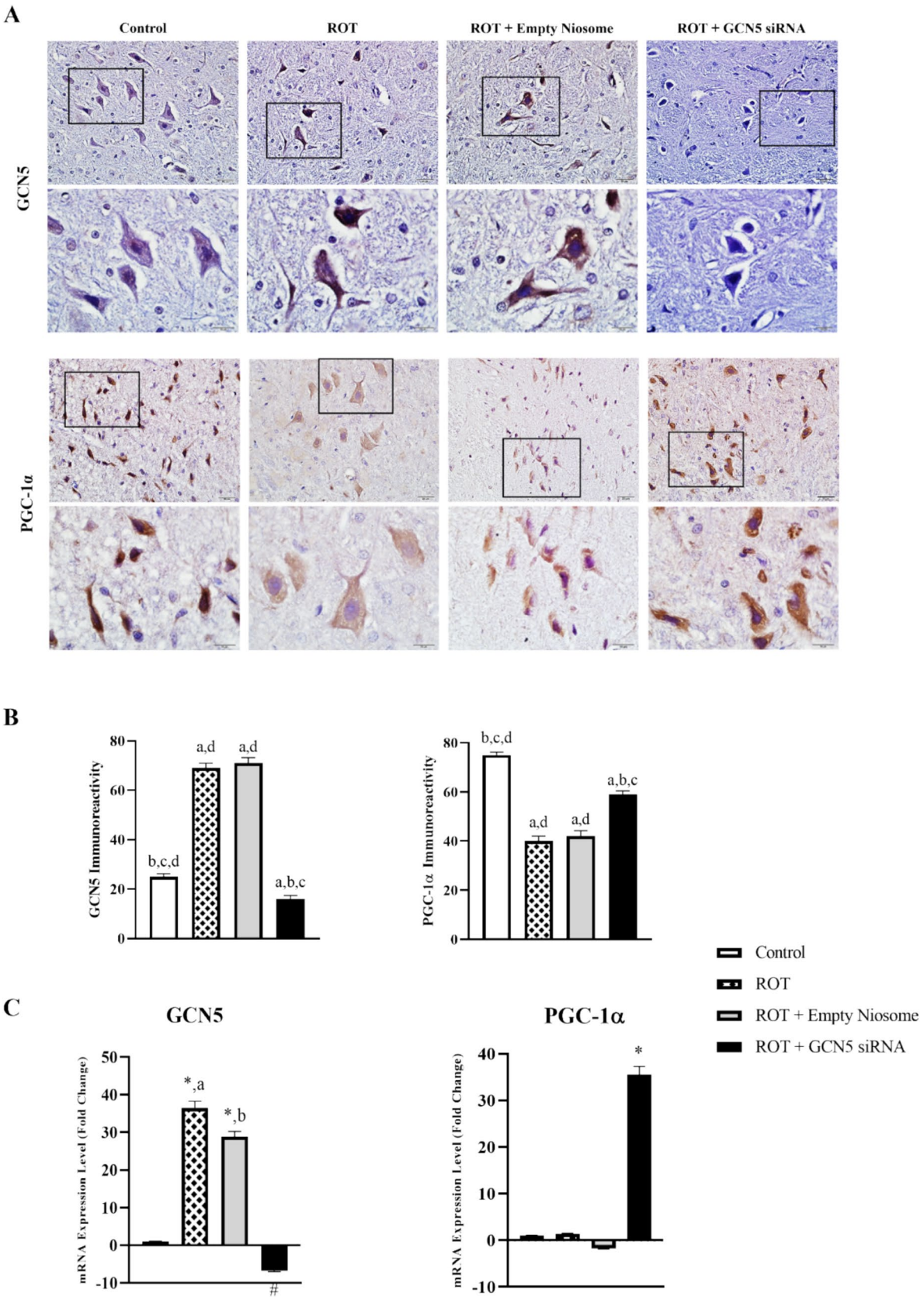
A
Control
ROT
ROT + Empty Niosome
ROT + GCN5 siRNA
GCN5
PGC-1α
B
GCN5 Immunoreactivity
b,c,d
a,d
a,d
a,b,c
PGC-1α Immunoreactivity
b,c,d
a,d
a,d
a,b,c
Control
ROT
ROT + Empty Niosome
ROT + GCN5 siRNA
C
GCN5
mRNA Expression Level (Fold Change)
*,a
*,b
#
PGC-1α
mRNA Expression Level (Fold Change)
*

◂**Fig. 6** Representative IHC images illustrating relative expression patterns of GCN5 and PGC-1α in the substantia nigra pars compacta (A). Rotenone-treated groups exhibited a marked increase in GCN5 immunoreactivity, particularly within dopaminergic neurons, accompanied by a noticeable reduction in PGC-1α expression. In contrast, the ROT + GCN5–siRNA group demonstrated a substantial decrease in GCN5 staining intensity, indicating successful gene silencing (B). RT-qPCR analysis (C) supported these findings, revealing elevated GCN5 mRNA levels in the ROT and ROT + Empty Niosome groups compared to Control, while a pronounced downregulation was observed in the siRNA-treated group. Notably, PGC-1α mRNA expression was significantly upregulated in the ROT + GCN5–siRNA group, further confirming the regulatory relationship between GCN5 suppression and PGC-1α activation. a: Significant difference compared to the Control group ($p < 0.0001$). b: Significant difference compared to the ROT group ($p < 0.0001$). c: Significant difference compared to the ROT + Empty Niosome group ($p < 0.0001$). d: Significant difference compared to the ROT + GCN5–siRNA group ($p < 0.0001$). d: Significant difference compared to the ROT + GCN5–siRNA group ($p < 0.0001$). *: Significant increase compared to the control group ($p < 0.0001$). #: Significant decrease compared to the control group ($p < 0.0001$)

Discussion

Current epidemiological data indicate that PD affects approximately 8.5 million individuals worldwide. Despite being identified nearly two centuries ago, its etiology remains incompletely understood [54, 55]. However, clinical and preclinical evidence suggests that multiple biological mechanisms—including oxidative stress, the accumulation of reactive oxygen species, neuroinflammation, endoplasmic reticulum stress, and mitochondrial dysfunction—play a critical role in the pathogenesis of PD by contributing directly or indirectly to the degeneration of dopaminergic neurons [56]. Although substantial progress has been made in elucidating these mechanisms, a definitive cure for PD remains elusive [57]. Current treatment strategies, primarily centered around levodopa administration and dopamine receptor agonists, are limited to symptomatic relief and often lead to undesirable side effects with prolonged use [58]. This underscores the urgent need for innovative preclinical and clinical investigations focused on targeting the molecular underpinnings of PD in order to develop more effective therapeutic approaches.

RNA interference (RNAi), which involves the silencing of specific genes through complementary nucleic acids such as small interfering RNAs (siRNAs), represents a promising avenue for personalized therapeutic approaches in PD [59]. However, a major obstacle in the clinical translation of siRNA-based therapies is the limited efficiency of gene silencing, largely due to enzymatic degradation, phagocytic clearance, cellular uptake barriers, and immune responses elicited by the siRNA molecules [60]. To overcome these challenges, the incorporation of delivery platforms is essential in both in vitro and in vivo applications to ensure the stability and intracellular transport of siRNAs [61].

Niosomes—vesicular nanocarriers structurally analogous to liposomes and formed by the self-assembly of non-ionic surfactants—have gained significant attention as delivery vehicles [62]. Preclinical investigations have shown that niosomes can enhance the bioavailability of drugs administered via subcutaneous, intravenous, oral, or transdermal routes, while also mitigating adverse effects [63, 64]. Importantly, further evidence indicates that niosomes are capable of encapsulating biologically fragile molecules such as siRNAs and facilitating their transport across the blood–brain barrier [23, 65]. Their biocompatibility and biodegradability further enhance their potential for safe siRNA delivery [66]. In the context of PD therapy, the therapeutic efficacy of targeted delivery systems is strongly influenced by the physicochemical properties of the nanocarriers. Key parameters such as particle size, surface charge, and morphology are critical not only for enhancing therapeutic outcomes but also for reducing off-target effects, and they also govern biodistribution, pharmacokinetics, and systemic clearance [67]. While intravenous administration is a widely used route for improving siRNA bioavailability, interactions with blood components, including plasma proteins and immune cells, remain significant limitations. Nanoparticles with high positive zeta potential or large diameters are more prone to rapid clearance by the reticuloendothelial system (RES) through opsonization and phagocytosis [68, 69]. Furthermore, cationic nanoparticles may exert cytotoxic effects, particularly at the level of the blood–brain barrier [70]. Conversely, although smaller nanoparticles are less susceptible to RES-mediated clearance, they may offer limited drug loading capacity and pose cytotoxic risks due to high surface energy. Among various particle geometries, spherical nanocarriers offer practical advantages for targeted delivery due to their ease of uniform fabrication and surface functionalization [67]. Collectively, these findings highlight the suitability of niosomes for siRNA delivery in PD treatment owing to their tunable physicochemical properties. Building upon this foundation, the present study provides preclinical evidence supporting the therapeutic utility of niosome–siRNA complexes in a rotenone-induced PD model. In vivo imaging system (IVIS) analysis demonstrated that the administered niosome–siRNA complex successfully reached the brain within 5 h post-injection and remained detectable in circulation beyond 24 h, confirming its potential for in vivo gene silencing. In addition, molecular analyses revealed a significant downregulation of GCN5 mRNA and immunoreactivity in the midbrain tissues of PD-model animals treated with the complex, underscoring the effectiveness of this delivery system in targeting disease-relevant genes.

Cumulative scientific research over the years indicates that the majority of PD cases are of sporadic origin [71]. Accordingly, the present study employed a rotenone-induced

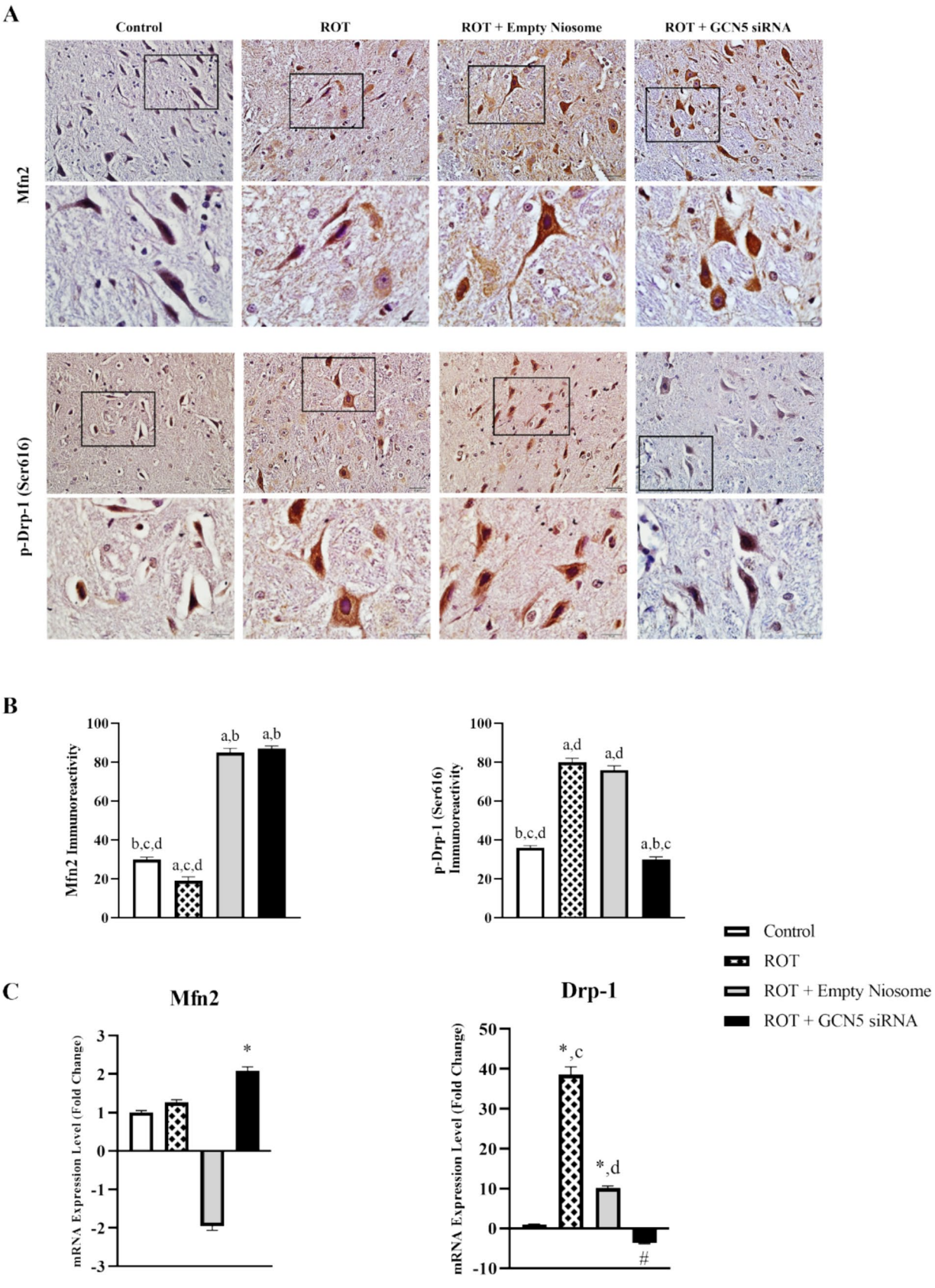
A
Control
ROT
ROT + Empty Niosome
ROT + GCN5 siRNA
Mfn2
p-Drp-1 (Ser616)
B
Mfn2 Immunoreactivity
b,c,d
a,c,d
a,b
a,b
p-Drp-1 (Ser616) Immunoreactivity
b,c,d
a,d
a,d
a,b,c
Control
ROT
ROT + Empty Niosome
ROT + GCN5 siRNA
C
Mfn2
mRNA Expression Level (Fold Change)
*
Drp-1
mRNA Expression Level (Fold Change)
*,c
*,d
#

◂**Fig. 7** Representative IHC images showing relative expression patterns of Mfn2 and Drp-1 in the SNpc. Rotenone-treated groups exhibited a marked increase in Drp-1 immunoreactivity, particularly in dopaminergic neurons, accompanied by a substantial decrease in Mfn2 expression (**A**). In contrast, the ROT + GCN5 siRNA group showed significantly reduced Drp-1 staining intensity, whereas Mfn2 immunoreactivity was relatively preserved (**B**). RT-qPCR analysis supported these observations, revealing elevated Mfn2 mRNA levels in the ROT and ROT + Empty Niosome groups compared to the Control. Notably, Drp-1 mRNA expression was significantly downregulated in the ROT + GCN5 siRNA group, further supporting a regulatory link between GCN5 silencing and PGC-1α-mediated mitochondrial dynamics (**C**). a: Significant difference compared to the Control group ($p < 0.0001$). b: Significant difference compared to the ROT group ($p < 0.0001$). c: Significant difference compared to the ROT + Empty Niosome group ($p < 0.0001$). d: Significant difference compared to the ROT + GCN5–siRNA group ($p < 0.0001$). d: Significant difference compared to the ROT + GCN5–siRNA group ($p < 0.0001$). *: Significant increase compared to the control group ($p < 0.0001$). #: Significant decrease compared to the control group ($p < 0.0001$)

sporadic PD model to investigate the effects of GCN5 gene silencing in vivo.

Rotenone, a mitochondrial complex I inhibitor, induces oxidative stress and mitochondrial dysfunction, which collectively lead to the degeneration of dopaminergic neurons. Furthermore, rotenone has been shown to cross the BBB via dopamine transporters and to promote α-syn aggregation and LB formation in the substantia SNpc [72]. For instance, Nie et al. demonstrated that chronic administration of rotenone (2 mg/kg/day for 35 days) resulted in a notable loss of TH-positive neurons in the SNpc and elevated α-syn expression levels in rats [73]. Given that TH is a reliable marker for dopaminergic neurons and α-syn accumulation is a hallmark of PD pathology [74] rotenone is widely accepted as a robust agent for modeling sporadic PD. Consistent with previous studies, our findings confirmed the successful induction of PD pathology, as evidenced by a reduction in TH-positive cells and increased α-syn immunoreactivity in the midbrain tissues of rotenone-treated rats. Importantly, treatment with the niosome-formulated siRNA targeting GCN5 significantly increased both the number of TH-positive neurons and TH expression levels when compared to the ROT and ROT + Empty Niosome groups, suggesting a neuroprotective effect of GCN5 silencing on dopaminergic neurons. Supporting these observations, Fan et al. demonstrated that pharmacological inhibition of GCN5 using MB-3 protected against MPP^+-induced toxicity in SH-SY5Y neuroblastoma cells [19]. These two parallel results suggest that GCN5 may be a potential therapeutic target in PD.

Under physiological conditions, α-syn regulates neurotransmitter trafficking; however, in PD, post-translational modifications—such as acetylation—alter its biochemical properties, promoting misfolding and aggregation into prefibrillar and fibrillar structures [75, 76]. These fibrillar α-syn aggregates form the core of LB, a pathological hallmark of PD, and ultimately contribute to progressive neuronal degeneration [76, 77]. Moreover, intracellular α-syn aggregates have been shown to exhibit a high affinity for histone H3 regions that are hyperacetylated by HATs. This interaction exacerbates α-syn aggregation, ultimately contributing to dopaminergic neuronal damage [78]. This body of literature is consistent with our experimental results, which demonstrated a marked reduction in α-syn mRNA and immunoreactivity levels in the group subjected to GCN5 gene knockdown, a gene known as the first histone acetyltransferase identified in mammals, compared to other groups treated with rotenone. Furthermore, histopathological evaluations revealed fewer LB-like inclusions in the midbrain tissue of the ROT + GCN5 siRNA group relative to other rotenone-exposed groups, suggesting that GCN5 knockdown may slow or suppress α-syn aggregation. Supporting this, behavioral assessments showed significantly reduced histopathological alterations in the midbrain, improved locomotor activity, and lower catalepsy scores in the ROT + GCN5 siRNA group compared to the other rotenone-treated groups. Considering previous reports that link locomotor deficits in rotenone-induced PD models to LB-like inclusions and other midbrain neuropathologies [79], our findings suggest that GCN5 gene silencing may exert a neuroprotective effect on dopaminergic neurons and contribute to the observed functional recovery. A previous study demonstrated that histone acetylation levels are elevated in postmortem brain tissue of PD patients and that inhibition of histone acetyltransferases using garcinol attenuates MPTP-induced neuronal loss [80], thereby lending further support to the preceding assumption.

Recent clinical and preclinical studies provide growing evidence that oxidative stress—resulting from decreased antioxidant enzyme activity and increased levels of lipid peroxidation products—contributes to the pathogenesis of PD by promoting mitochondrial dysfunction and α-syn accumulation in dopaminergic neurons [81]. For instance, a 2023 study by Vastegani et al. reported that in a rotenone-induced PD model, decreased activity of the antioxidant enzyme SOD alongside elevated levels of MDA, a key lipid peroxidation product, led to α-syn accumulation in the midbrain and impaired locomotor activity in rats [82]. Consistent with these findings, our biochemical analyses revealed a significant reduction in SOD activity and a marked increase in MDA levels in the midbrain tissues of rats treated with rotenone. On the other hand, in the group subjected to GCN5 gene knockdown, SOD activity was significantly elevated, whereas MDA levels were significantly reduced compared to the other rotenone-treated groups. When these biochemical findings are considered in conjunction with histopathological evaluations, behavioral test outcomes, and immunohistochemical findings of TH—a key marker of dopaminergic

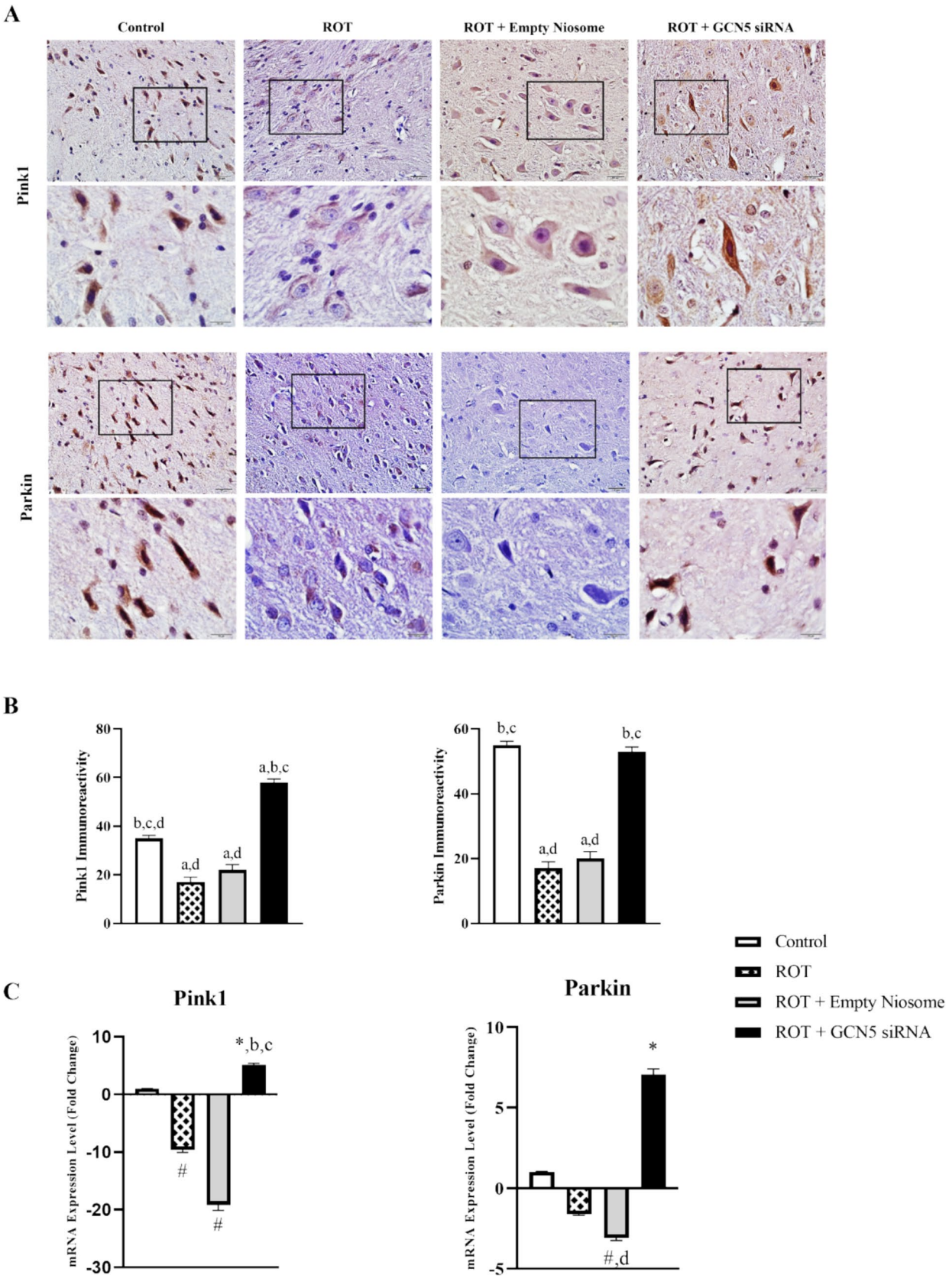
A
Control
ROT
ROT + Empty Niosome
ROT + GCN5 siRNA
Pink1
Parkin
B
Pink1 Immunoreactivity
80
60
40
20
0
b,c,d
a,d
a,d
a,b,c
Parkin Immunoreactivity
60
40
20
0
b,c
a,d
a,d
b,c
C
Pink1
mRNA Expression Level (Fold Change)
10
0
-10
-20
-30
#
#
*,b,c
Parkin
mRNA Expression Level (Fold Change)
10
5
0
-5
#,d
*
Control
ROT
ROT + Empty Niosome
ROT + GCN5 siRNA

◂**Fig. 8** Representative IHC images illustrating relative expression patterns of PINK1 and Parkin in the SNpc (**A**). Rotenone-treated groups exhibited a noticeable reduction in both PINK1 and Parkin immunoreactivity. In contrast, the ROT + GCN5 siRNA group demonstrated higher expression intensities of both proteins compared to other experimental groups (**B**). RT-qPCR analysis confirmed these findings, revealing elevated Pink1 and Parkin mRNA levels in the ROT and ROT + Empty Niosome groups relative to the Control (**C**). These results support the hypothesis that GCN5 silencing exerts neuroprotective effects by modulating the mitophagy pathway through regulation of Pink1 and Parkin expression. a: Significant difference compared to the Control group ($p < 0.0001$). b: Significant difference compared to the ROT group ($p < 0.0001$). c: Significant difference compared to the ROT + Empty Niosome group ($p < 0.0001$). d: Significant difference compared to the ROT + GCN5–siRNA group ($p < 0.0001$). d: Significant difference compared to the ROT + GCN5–siRNA group ($p < 0.0001$). *: Significant increase compared to the control group ($p < 0.0001$). #: Significant decrease compared to the control group ($p < 0.0001$)

neurons—it can be inferred that GCN5 gene silencing exerts a neuroprotective effect by enhancing antioxidant defense mechanisms in the midbrain. Furthermore, it demonstrated that GCN5 overexpression in a mouse vascular endothelial cell line cultured under hyperglycemic conditions induced oxidative stress [15]. These findings support the notion that siRNA-mediated GCN5 knockdown may enhance antioxidant defense by suppressing GCN5 expression and thus mitigate oxidative stress at the cellular level.

Mitochondrial dysfunction is central to PD pathogenesis, and a suite of interrelated genes—including Parkin, Pink1, Drp-1, Mfn2, and PGC-1α—play key roles in maintaining mitochondrial health [83]. Under normal conditions, PINK1 accumulates on depolarized mitochondria, recruiting the E3 ubiquitin ligase Parkin to initiate mitophagy by ubiquitinating outer-membrane proteins; mutations in either PINK1 or Parkin disrupt this quality control, leading to accumulation of damaged mitochondria and enhanced oxidative stress in dopaminergic neurons [84, 85]. Parkin also targets the transcriptional repressor PARIS for degradation, thereby enabling PGC-1α activation, which drives mitochondrial biogenesis via NRF-1/2 and TFAM; loss of Parkin function consequently reduces PGC-1α signaling, diminishing mitochondrial renewal and antioxidant capacity [86]. Also, Parkin-mediated ubiquitination of Mfn1/2 prevents damaged mitochondria from re-fusing, while Drp-1-mediated fission facilitates mitochondrial segregation; disruptions in this balance, often seen in PD, exacerbate neuronal oxidative damage [87]. Moreover, PGC-1α not only orchestrates biogenesis but also enhances the expression of antioxidant enzymes, thereby reducing ROS levels; its deficiency has been linked to increased susceptibility of dopaminergic neurons to oxidative stress [86]. In addition, PGC-1α increases mitochondrial fusion by regulating the expression level of Drp-1, thereby contributing to the alleviation of neurodegeneration [88]. Collectively, impairments in mitophagy (Pink1/Parkin), defective dynamics (Mfn2/Drp-1), and suppressed biogenesis (PGC-1α) converge to drive mitochondrial dysfunction, elevate ROS production, and promote dopaminergic cell death—the hallmark deficits of PD [83]. IHC and RT-qPCR analyses demonstrated that GCN5 gene silencing modulates the expression levels of key regulators of mitochondrial homeostasis at both mRNA and immunoreactivity levels. In the ROT and ROT + Empty Niosome groups, upregulation of GCN5 was accompanied by a significant increase in Drp-1 and a notable decrease in PGC-1α expression when compared to the Control and ROT + GCN5 siRNA groups. Conversely, in the GCN5 knockdown group, GCN5 and Drp-1 levels were significantly reduced, while PGC-1α expression was markedly elevated. These results align with prior findings indicating that GCN5 suppresses mitochondrial biogenesis and quality control by acetylating and inhibiting PGC-1α [89]. Additionally, while Drp-1 promotes mitochondrial fission and axonal damage, PGC-1α enhances mitochondrial fusion by downregulating Drp-1, thereby exerting a neuroprotective effect [88]. Collectively, our findings suggest that rotenone-induced upregulation of GCN5 may impair PGC-1α activity, leading to Drp-1-mediated neuronal damage, whereas GCN5 silencing may enhance PGC-1α function and mitigate dopaminergic neurotoxicity. Moreover, our data reveal that GCN5 knockdown significantly alters the expression of mitophagy-related genes Parkin, PINK1, and Mfn2. In the ROT and Empty Niosome groups, expression of these genes was markedly downregulated, while their levels were significantly elevated in the ROT + GCN5 siRNA group compared to both rotenone-treated and control animals. These findings imply that silencing of GCN5 may enhance Parkin/PINK1/Mfn2-mediated mitophagy and contribute to dopaminergic neuronal protection in PD. A study by Scott et al. demonstrated that GCN5L1 exerts a suppressive role in regulating mitochondrial biogenesis and mitophagy in mouse embryonic fibroblasts, as evidenced by enhanced mitochondrial biogenesis and mitophagy in GCN5L1$^{-/-}$ mutant cells [17]. These findings support our conclusion that GCN5 gene knockdown may promote mitophagy and exert neuroprotective effects in dopaminergic neurons. However, contrasting evidence from a more recent study showed that GCN5 overexpression protected SH-SY5Y neuroblastoma cells from α-synuclein–induced apoptosis [90]. This discrepancy highlights the complexity of GCN5's role in dopaminergic neuron homeostasis and PD pathogenesis, underscoring the need for further studies to explore its function across different biological contexts.

In summary, GCN5 gene knockdown via a siRNA–niosomal complex was found to exert a neuroprotective effect on midbrain dopaminergic neurons by restoring antioxidant system activity and modulating the expression of key molecules involved in mitochondrial homeostasis. The observed

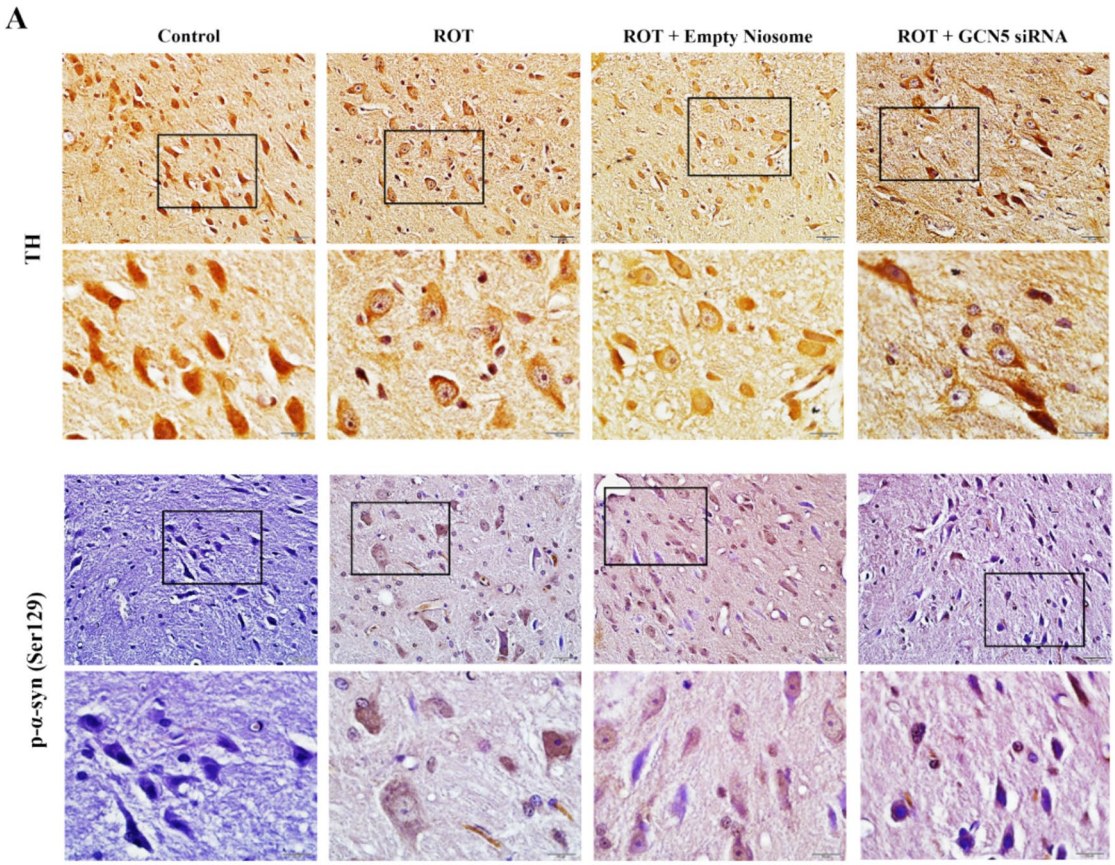
A
Control
ROT
ROT + Empty Niosome
ROT + GCN5 siRNA
TH
p-α-syn (Ser129)

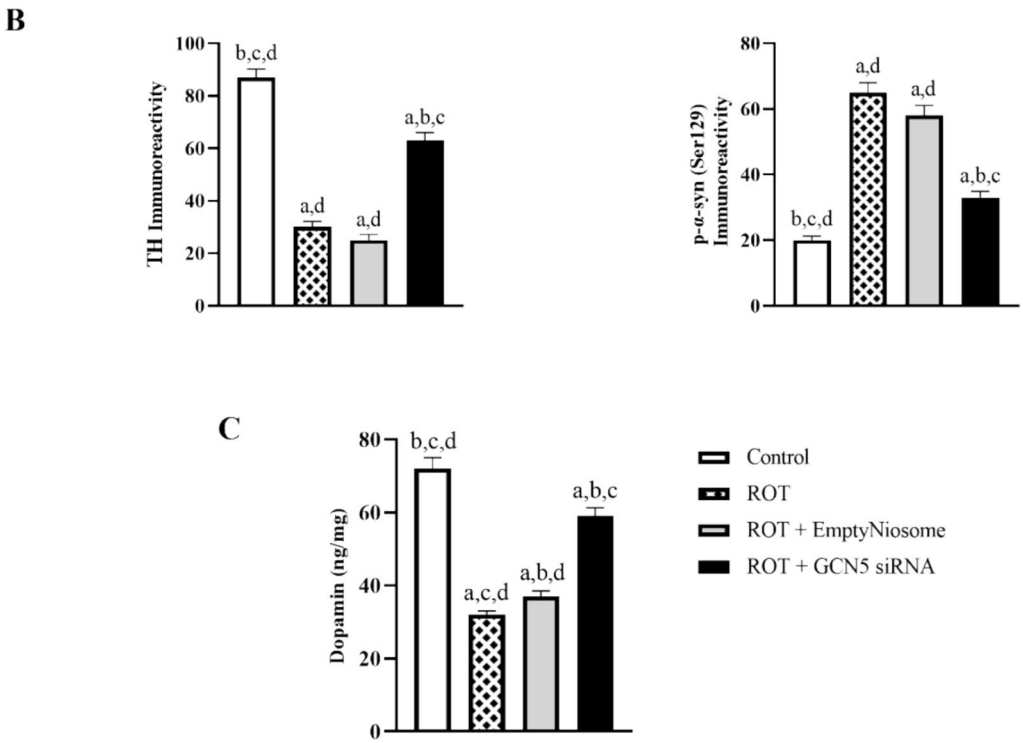
B
TH Immunoreactivity
100
80
60
40
20
0
b,c,d
a,d
a,d
a,b,c
p-α-syn (Ser129) Immunoreactivity
80
60
40
20
0
b,c,d
a,d
a,d
a,b,c

C
Dopamin (ng/mg)
80
60
40
20
0
b,c,d
a,c,d
a,b,d
a,b,c
Control
ROT
ROT + EmptyNiosome
ROT + GCN5 siRNA

◂**Fig. 9** Representative micrographs showing TH and α-syn immunoreactivity in the SNpc (A). TH expression was markedly reduced in rotenone-injected groups compared to the Control group; however, TH levels remained relatively higher in the ROT + GCN5 siRNA group than in the other rotenone-treated cohorts. In contrast, α-syn immunoreactivity levels were elevated in the ROT and ROT + Empty Niosome groups, whereas GCN5 silencing via siRNA treatment led to a significant reduction in α-syn expression (B). These alterations in immunoreactivity expression were further supported by ELISA quantification of dopamine levels, a key biomarker strongly associated with PD (C). a: Significant difference compared to the Control group ($p < 0.0001$). b: Significant difference compared to the ROT group ($p < 0.0001$). c: Significant difference compared to the ROT + Empty Niosome group ($p < 0.0001$). d: Significant difference compared to the ROT + GCN5–siRNA group ($p < 0.0001$). d: Significant difference compared to the ROT + GCN5–siRNA group ($p < 0.0001$)

protective effects appear to be mediated by the upregulation of PGC-1α following GCN5 knockdown, which regulates the expression of genes related to mitochondrial biogenesis, mitophagy, and oxidative stress responses. Previous studies have shown that PGC-1α modulates mitophagy through PINK1, Parkin, and Mfn2, mitochondrial dynamics via Drp-1, and antioxidant defense through increased enzymatic activity [91]. Additionally, GCN5 has been reported to negatively regulate PGC-1α activity [16], supporting this proposed mechanism. Nevertheless, further studies exploring alternative molecular pathways are warranted to fully elucidate the neuroprotective role of GCN5 silencing in dopaminergic neurons.

Limitations of the Study

While this study confirmed the successful delivery of niosome–siRNA complexes to the brain, several key analyses that could have provided additional mechanistic insights were not feasible due to limited technical capacity and financial resources. Transcriptome-wide approaches such as RNA sequencing, which could have revealed broader regulatory networks impacted by GCN5 gene silencing, were not conducted. Similarly, antibodies required to detect acetylated variants of proteins could not be procured. Additional biophysical assessments—such as gel electrophoresis-based retardation assays to evaluate siRNA binding efficiency, or Fourier-transform infrared spectroscopy (FTIR) to examine molecular interactions between siRNA and niosomal components—were also not performed. Moreover, hemocompatibility tests, including the hemolysis assay commonly used to assess the safety of intravenous nanocarrier administration, were omitted for similar logistical reasons. These limitations, though not affecting the central conclusions of the study, highlight important considerations for future research aiming to fully characterize siRNA-loaded delivery systems.

The absence of Western Blot validation represents a limitation of the present study; however, the use of multiple complementary high-cost experimental approaches necessitated prioritization of analyses within the available resources.

Supplementary Information The online version contains supplementary material available at https://doi.org/10.1007/s12035-026-05700-7.

Acknowledgements This article is based on Dr. Gökçe Ceren Kuşçu's PhD thesis. We gratefully acknowledge the valuable scientific and technical support received from Professor Emin İlker Medine and Mr. Tuncer Gürel.

Author Contribution GCK, ÇG, and AY undertook the study design. ÇG, GCK, and AB, undertook the animal experiments. ET undertook the niosome synthesis. GCK, ÇG, and AB undertook the histological experiments. CG and NÜKY undertook the biochemical experiments. EŞ undertook the IVIS analysis. ÇBA and ÖSG undertook the molecular experiments. ÇG, GCK, EŞ, and ET assisted with the statistical analysis. GCK undertook the creation of graphs and figures. ÇG and AY wrote the final manuscript. The manuscript was read and approved by all named authors.

Funding This study was supported by Ege University Scientific Research Foundation (grant number: TDK-2021–23271 to Altuğ Yavaşoğlu).

Data Availability The datasets generated during and/or analysed during the current study are available from the corresponding author on reasonable request.

Declarations

Ethics Approval The experimental protocol was evaluated and approved by Ege University, Local Ethics Committee for Animal Experiments (Approval No/Approval Date: 2021- 040/June 23, 2021).

Conflict of interest The authors declare no competing interests.

References

1. Bej E, Cesare P, Volpe AR et al (2024) Oxidative stress and neurodegeneration: insights and therapeutic strategies for Parkinson's disease. Neurol Int 16:502–517. https://doi.org/10.3390/NEUROLINT16030037
2. Merghany RM, El-Sawi SA, Naser AFA et al (2025) *Pelargonium graveolens* attenuates rotenone-induced Parkinson's disease in a rat model: role of MAO-B inhibition and in silico study. Mol Neurobiol. https://doi.org/10.1007/S12035-025-04727-6
3. Calabresi P, Mechelli A, Natale G et al (2023) Alpha-synuclein in Parkinson's disease and other synucleinopathies: from overt neurodegeneration back to early synaptic dysfunction. Cell Death Dis 14(3):1–16. https://doi.org/10.1038/s41419-023-05672-9
4. Henrich MT, Oertel WH, Surmeier DJ, Geibl FF (2023) Mitochondrial dysfunction in Parkinson's disease – a key disease hallmark with therapeutic potential. Mol Neurodegener 181(18):1–20. https://doi.org/10.1186/S13024-023-00676-7
5. Moon HE, Paek SH (2015) Mitochondrial dysfunction in Parkinson's disease. Exp Neurobiol 24:103–116. https://doi.org/10.5607/en.2015.24.2.103

6. Tryphena KP, Anuradha U, Kumar R et al (2023) Understanding the involvement of microRNAs in mitochondrial dysfunction and their role as potential biomarkers and therapeutic targets in Parkinson's disease. J Alzheimers Dis 94:S187–S202. https://doi.org/10.3233/JAD-220449
7. Miziak P, Baran M, Borkiewicz L et al (2024) Acetylation of histone H3 in cancer progression and prognosis. Int J Mol Sci 25(20):10982. https://doi.org/10.3390/IJMS252010982
8. Zhang X, Zhou Y, Liu Y et al (2024) Research progress on the mechanism and function of histone acetylation regulating the interaction between pathogenic fungi and plant hosts. J Fungi 10:522. https://doi.org/10.3390/JOF10080522
9. Liu R, Wu J, Guo H et al (2023) Post-translational modifications of histones: mechanisms, biological functions, and therapeutic targets. MedComm 4:e292. https://doi.org/10.1002/mco2.292
10. Kabir F, Atkinson R, Cook AL et al (2023) The role of altered protein acetylation in neurodegenerative disease. Front Aging Neurosci 14:1025473. https://doi.org/10.3389/FNAGI.2022.1025473
11. Gebremedhin KG, Rademacher DJ (2016) Histone H3 acetylation in the postmortem Parkinson's disease primary motor cortex. Neurosci Lett 627:121–125. https://doi.org/10.1016/J.NEULET.2016.05.060
12. Sugeno N, Jäckel S, Voigt 1A et al (2016) α-Synuclein enhances histone H3 lysine-9 dimethylation and H3K9me2-dependent transcriptional responses. Sci Reports 61 6:1–11. https://doi.org/10.1038/srep36328
13. Toker L, Tran GT, Sundaresan J et al (2021) Genome-wide histone acetylation analysis reveals altered transcriptional regulation in the Parkinson's disease brain. Mol Neurodegener 16:1–20. https://doi.org/10.1186/S13024-021-00450-7/FIGURES/6
14. Ryu YK, Park HY, Go J et al (2018) Effects of histone acetyltransferase inhibitors on l-DOPA-induced dyskinesia in a murine model of Parkinson's disease. J Neural Transm 125:1319–1331. https://doi.org/10.1007/S00702-018-1902-4/FIGURES/7
15. Xiao HT, Jin J, Zheng ZG (2023) Emerging role of GCN5 in human diseases and its therapeutic potential. Biomed Pharmacother 165:114835. https://doi.org/10.1016/J.BIOPHA.2023.114835
16. Mutlu B, Puigserver P (2021) GCN5 acetyltransferase in cellular energetic and metabolic processes. Biochimica et Biophysica Acta (BBA) - Gene Regulatory Mechanisms 1864:194626. https://doi.org/10.1016/J.BBAGRM.2020.194626
17. Scott I, Webster BR, Chan CK et al (2014) GCN5-like protein 1 (GCN5L1) controls mitochondrial content through coordinated regulation of mitochondrial biogenesis and mitophagy. J Biol Chem 289:2864–2872. https://doi.org/10.1074/JBC.M113.521641
18. Wareski P, Vaarmann A, Choubey V et al (2009) PGC-1α and PGC-1β regulate mitochondrial density in neurons. J Biol Chem 284:21379–21385. https://doi.org/10.1074/jbc.M109.018911
19. Fan F, Li S, Wen Z et al (2020) Regulation of PGC-1α mediated by acetylation and phosphorylation in MPP+ induced cell model of Parkinson's disease. Aging Albany NY 12:9461–9474. https://doi.org/10.18632/aging.103219
20. Bobbin ML, Rossi JJ (2016) RNA interference (RNAi)-based therapeutics: delivering on the promise? Annu Rev Pharmacol Toxicol 56:103–122. https://doi.org/10.1146/annurev-pharmtox-010715-103633
21. Lin J-Y, Xie C-L, Zhang S-F et al (2017) Current experimental studies of gene therapy in Parkinson's disease. Front Aging Neurosci 9:126. https://doi.org/10.3389/fnagi.2017.00126
22. Yao X-Y, Cao B-E, Liu J-Y et al (2024) Microglial melatonin receptor 1 degrades pathological alpha-synuclein through activating LC3-associated phagocytosis *in vitro*. CNS Neurosci Ther 30:e70088. https://doi.org/10.1111/cns.70088
23. Gharbavi M, Amani J, Kheiri-Manjili H et al (2018) Niosome: a promising nanocarrier for natural drug delivery through blood-brain barrier. Adv Pharmacol Sci. https://doi.org/10.1155/2018/6847971
24. Ge X, Wei M, He S, Yuan WE (2019) Advances of non-ionic surfactant vesicles (niosomes) and their application in drug delivery. Pharmaceutics 11:55. https://doi.org/10.3390/PHARMACEUTICS11020055
25. Chen Y, Dai R, Cheng M et al (2024) Status and role of the ubiquitin–proteasome system in renal fibrosis. Biomed Pharmacother 178:117210. https://doi.org/10.1016/J.BIOPHA.2024.117210
26. Revankar AA, Patil AS, Karishetti R et al (2024) Enhanced bioavailability of quercetin-loaded niosomal in situ gel for the management of Parkinson's disease. Front Pharmacol. https://doi.org/10.3389/FPHAR.2024.1519649
27. Gunay MS, Ozer AY, Erdogan S et al (2017) Development of nanosized, pramipexole-encapsulated liposomes and niosomes for the treatment of Parkinson's disease. J Nanosci Nanotechnol 17:5155–5167. https://doi.org/10.1166/jnn.2017.13799
28. Weinert M, Selvakumar T, Tierney TS, Alavian KN (2015) Isolation, culture and long-term maintenance of primary mesencephalic dopaminergic neurons from embryonic rodent brains. J Vis Exp 52475. https://doi.org/10.3791/52475
29. Daadi MM, Grueter BA, Malenka RC et al (2012) Dopaminergic neurons from midbrain-specified human embryonic stem cell-derived neural stem cells engrafted in a monkey model of Parkinson's disease. PLoS One 7:e41120. https://doi.org/10.1371/journal.pone.0041120
30. Liga S, Paul C, Moacă EA, Péter F (2024) Niosomes: composition, formulation techniques, and recent progress as delivery systems in cancer therapy. Pharmaceutics 16(2):223. https://doi.org/10.3390/PHARMACEUTICS16020223
31. Paecharoenchai O, Teng L, Yung BC et al (2013) Nonionic surfactant vesicles for delivery of RNAi therapeutics. Nanomedicine 8:1865–1873. https://doi.org/10.2217/NNM.13.155
32. Moulahoum H, Sanli S, Timur S, Zihnioglu F (2019) Potential effect of carnosine encapsulated niosomes in bovine serum albumin modifications. Int J Biol Macromol 137:583–591. https://doi.org/10.1016/J.IJBIOMAC.2019.07.003
33. Tut E, Guldu OK, Medine EI (2024) Antitumor properties of bromelain loaded trastuzumab conjugated niosomes in HER2+ breast cancer cells. J Drug Deliv Sci Technol 101:106243. https://doi.org/10.1016/J.JDDST.2024.106243
34. Huang Y, Chen J, Chen X et al (2008) PEGylated synthetic surfactant vesicles (niosomes): novel carriers for oligonucleotides. J Mater Sci Mater Med 19:607–614. https://doi.org/10.1007/s10856-007-3193-4
35. Endres T, Zheng M, Beck-Broichsitter M, Kissel T (2012) Lyophilised ready-to-use formulations of PEG-PCL-PEI nanocarriers for siRNA delivery. Int J Pharm 428:121–124. https://doi.org/10.1016/J.IJPHARM.2012.03.003
36. Thabet Y, Elsabahy M, Eissa NG (2022) Methods for preparation of niosomes: a focus on thin-film hydration method. Methods 199:9–15. https://doi.org/10.1016/J.YMETH.2021.05.004
37. Hemati M, Haghiralsadat F, Yazdian F et al (2019) Development and characterization of a novel cationic PEGylated niosome-encapsulated forms of doxorubicin, quercetin and siRNA for the treatment of cancer by using combination therapy. Artif Cells Nanomed Biotechnol 47:1295–1311. https://doi.org/10.1080/21691401.2018.1489271
38. Cooper JM, Wiklander PBO, Nordin JZ et al (2014) Systemic exosomal siRNA delivery reduced alpha-synuclein aggregates in brains of transgenic mice. Mov Disord 29:1476–1485. https://doi.org/10.1002/mds.25978
39. Livak KJ, Schmittgen TD (2001) Analysis of relative gene expression data using real-time quantitative PCR and the 2(-Delta Delta C(T)) method. Methods 25:402–408. https://doi.org/10.1006/meth.2001.1262

40. du Percie Sert N, Hurst V, Ahluwalia A et al (2020) The ARRIVE guidelines 2.0: updated guidelines for reporting animal research. PLoS Biol 18:e3000410. https://doi.org/10.1371/journal.pbio.3000410
41. Chen Y, Zhang DQ, Liao Z et al (2015) Anti-oxidant polydatin (piceid) protects against substantia nigral motor degeneration in multiple rodent models of Parkinson's disease. Mol Neurodegener 10:1–14. https://doi.org/10.1186/1750-1326-10-4
42. Prut L, Belzung C (2003) The open field as a paradigm to measure the effects of drugs on anxiety-like behaviors: a review. Eur J Pharmacol 463:3–33. https://doi.org/10.1016/S0014-2999(03)01272-X
43. Sanberg PR (1980) Haloperidol-induced catalepsy is mediated by postsynaptic dopamine receptors. Nature 284:472–473. https://doi.org/10.1038/284472a0
44. Leslie J, Robinson SM, Oakley F, Luli S (2021) Non-invasive synchronous monitoring of neutrophil migration using whole body near-infrared fluorescence-based imaging. Sci Rep 11:1415. https://doi.org/10.1038/s41598-021-81097-8
45. Paxinos G, Watson C (2005) The rat brain in stereotaxic coordinates, Fifth Edit. Elsevier, San Diego, CA, USA
46. Young K, Morrison H (2018) Quantifying microglia morphology from photomicrographs of immunohistochemistry prepared tissue using ImageJ. J Vis Exp. https://doi.org/10.3791/57648
47. Rao X, Huang X, Zhou Z, Lin X (2013) An improvement of the 2ˆ(-delta delta CT) method for quantitative real-time polymerase chain reaction data analysis. Biostat Bioinforma Biomath 3:71–85
48. Wu Y, Ma S, Xia Y et al (2017) Loss of GCN5 leads to increased neuronal apoptosis by upregulating E2F1- and Egr-1-dependent BH3-only protein Bim. Cell Death Dis 8:e2570–e2570. https://doi.org/10.1038/cddis.2016.465
49. Ning XJ, Yan X, Wang YF et al (2018) Parkin deficiency elevates hepatic ischemia/reperfusion injury accompanying decreased mitochondrial autophagy, increased apoptosis, impaired DNA damage repair and altered cell cycle distribution. Mol Med Rep 18:5663–5668. https://doi.org/10.3892/mmr.2018.9606
50. Zhou L, Zhang L, Zhang Y et al (2019) PINK1 deficiency ameliorates cisplatin-induced acute kidney injury in rats. Front Physiol 10:1225. https://doi.org/10.3389/fphys.2019.01225
51. Son SH, Lee SM, Lee MH et al (2021) Omega-3 fatty acids upregulate SIRT1/3, activate PGC-1α via deacetylation, and induce Nrf1 production in 5/6 nephrectomy rat model. Mar Drugs. https://doi.org/10.3390/md19040182
52. Drummond MJ, Glynn EL, Lujan HL et al (2008) Gene and protein expression associated with protein synthesis and breakdown in paraplegic skeletal muscle. Muscle Nerve 37:505–513. https://doi.org/10.1002/mus.20976
53. Zhang Q, Chen S, Yu S et al (2016) Neuroprotective effects of pyrroloquinoline quinone against rotenone injury in primary cultured midbrain neurons and in a rat model of Parkinson's disease. Neuropharmacology 108:238–251. https://doi.org/10.1016/J.NEUROPHARM.2016.04.025
54. McDonald C, Gordon G, Hand A et al (2018) 200 years of Parkinson's disease: what have we learnt from James Parkinson? Age Ageing 47:209–214. https://doi.org/10.1093/ageing/afx196
55. Tassew TM, Xuan N, Chai B (2023) PDDS: a software for the early diagnosis of Parkinson's disease from MRI and DaT scan images using detection and segmentation algorithms. Biomed Signal Process Control 86:105140. https://doi.org/10.1016/j.bspc.2023.105140
56. Karvandi MS, Sheikhzadeh Hesari F, Aref AR, Mahdavi M (2023) The neuroprotective effects of targeting key factors of neuronal cell death in neurodegenerative diseases: the role of ER stress, oxidative stress, and neuroinflammation. Front Cell Neurosci 17:1105247. https://doi.org/10.3389/FNCEL.2023.1105247
57. Adam H, Gopinath SCBB, Md Arshad MK et al (2023) An update on pathogenesis and clinical scenario for Parkinson's disease: diagnosis and treatment. 3 Biotech 13:142. https://doi.org/10.1007/s13205-023-03553-8
58. Szunyogh S, Carroll E, Wade-Martins R (2025) Recent developments in gene therapy for Parkinson's disease. Mol Ther. https://doi.org/10.1016/J.YMTHE.2025.03.030
59. Li D, Mastaglia FL, Fletcher S, Wilton SD (2020) Progress in the molecular pathogenesis and nucleic acid therapeutics for Parkinson's disease in the precision medicine era. Med Res Rev 40:2650–2681. https://doi.org/10.1002/MED.21718
60. Tatiparti K, Sau S, Kashaw S, Iyer A (2017) SiRNA delivery strategies: a comprehensive review of recent developments. Nanomaterials 7:77. https://doi.org/10.3390/nano7040077
61. Dong Y, Siegwart DJ, Anderson DG (2019) Strategies, design, and chemistry in siRNA delivery systems. Adv Drug Deliv Rev 144:133–147. https://doi.org/10.1016/j.addr.2019.05.004
62. Lens M (2025) Niosomes as vesicular nanocarriers in cosmetics: characterisation, development and efficacy. Pharmaceutics 17:287. https://doi.org/10.3390/pharmaceutics17030287
63. Abdelrahman FE, Elsayed I, Gad MK et al (2017) Response surface optimization, ex vivo and in vivo investigation of nasal spanlastics for bioavailability enhancement and brain targeting of risperidone. Int J Pharm 530:1–11. https://doi.org/10.1016/j.ijpharm.2017.07.050
64. Zidan AS, Habib MJ (2014) Maximized mucoadhesion and skin permeation of anti-AIDS-loaded niosomal gels. J Pharm Sci 103:952–964. https://doi.org/10.1002/jps.23867
65. Yang C, Gao S, Song P et al (2018) Theranostic niosomes for efficient siRNA/microRNA delivery and activatable near-infrared fluorescent tracking of stem cells. ACS Appl Mater Interfaces 10:19494–19503. https://doi.org/10.1021/acsami.8b05513
66. Yasamineh S, Yasamineh P, Ghafouri Kalajahi H et al (2022) A state-of-the-art review on the recent advances of niosomes as a targeted drug delivery system. Int J Pharm 624:121878. https://doi.org/10.1016/j.ijpharm.2022.121878
67. Ding S, Khan AI, Cai X et al (2020) Overcoming blood–brain barrier transport: advances in nanoparticle-based drug delivery strategies. Mater Today 37:112–125. https://doi.org/10.1016/j.mattod.2020.02.001
68. Alexis F, Pridgen E, Molnar LK, Farokhzad OC (2008) Factors affecting the clearance and biodistribution of polymeric nanoparticles. Mol Pharm 5:505–515. https://doi.org/10.1021/mp800051m
69. Owens D III, Peppas N (2006) Opsonization, biodistribution, and pharmacokinetics of polymeric nanoparticles. Int J Pharm 307:93–102. https://doi.org/10.1016/j.ijpharm.2005.10.010
70. Lockman PR, Koziara JM, Mumper RJ, Allen DD (2004) Nanoparticle surface charges alter blood–brain barrier integrity and permeability. J Drug Target 12:635–641. https://doi.org/10.1080/10611860400015936
71. Tenchov R, Sasso JM, Zhou QA (2025) Evolving landscape of Parkinson's disease research: challenges and perspectives. ACS Omega 10:1864–1892. https://doi.org/10.1021/ACSOMEGA.4C09114/ASSET/IMAGES/MEDIUM/AO4C09114_0018.GIF
72. Pirunkaset E, Boonyarat C, Maneenet J et al (2024) Effect of diacetylcurcumin manganese complex on rotenone-induced oxidative stress, mitochondria dysfunction, and inflammation in the SH-SY5Y Parkinson's disease cell model. Molecules 29:957. https://doi.org/10.3390/MOLECULES29050957
73. Nie S, Ma K, Sun M et al (2019) 7,8-dihydroxyflavone protects nigrostriatal dopaminergic neurons from rotenone-induced neurotoxicity in rodents. Parkinsons Dis 2019:1–10. https://doi.org/10.1155/2019/9193534
74. Giráldez-Pérez RM, Antolín-Vallespín M, Muñoz MD, Sánchez-Capelo A (2014) Models of α-synuclein aggregation in

Parkinson's disease. Acta Neuropathol Commun 2:1–17. https://doi.org/10.1186/S40478-014-0176-9/FIGURES/1
75. Gao V, Briano JA, Komer LE, Burré J (2023) Functional and pathological effects of α-synuclein on synaptic SNARE complexes. J Mol Biol 435:167714. https://doi.org/10.1016/j.jmb.2022.167714
76. Picca A, Guerra F, Calvani R et al (2021) Mitochondrial dysfunction, protein misfolding and neuroinflammation in Parkinson's disease: roads to biomarker discovery. Biomolecules 11:1508. https://doi.org/10.3390/biom11101508
77. Li X, Wang W, Pan S et al (2024) Exploring heat shock proteins as therapeutic targets for Parkinson's disease. Biochem Pharmacol 230:116633. https://doi.org/10.1016/j.bcp.2024.116633
78. Rasheed M, Liang J, Wang C et al (2021) Epigenetic regulation of neuroinflammation in Parkinson's disease. Int J Mol Sci 22:4956. https://doi.org/10.3390/ijms22094956
79. Sherer TB, Betarbet R, Testa CM et al (2003) Mechanism of toxicity in rotenone models of Parkinson's disease. J Neurosci 23:10756–10764. https://doi.org/10.1523/JNEUROSCI.23-34-10756.2003
80. Park G, Tan J, Garcia G et al (2016) Regulation of histone acetylation by autophagy in Parkinson disease. J Biol Chem 291:3531–3540. https://doi.org/10.1074/jbc.M115.675488
81. Chakrabarti S, Bisaglia M (2023) Oxidative stress and neuroinflammation in Parkinson's disease: the role of dopamine oxidation products. Antioxidants. https://doi.org/10.3390/ANTIOX12040955
82. Moradi Vastegani S, Khoshnam SE, Ghafouri S et al (2023) Anethole attenuates motor dysfunctions, striatal neuronal activity deficiency and blood brain barrier permeability by decreasing striatal α-synuclein and oxidative stress in rotenone-induced Parkinson's disease of male rats. PLoS ONE 18:e0294612. https://doi.org/10.1371/JOURNAL.PONE.0294612
83. Gąssowska-Dobrowolska M, Olech-Kochańczyk G, Culmsee C, Adamczyk A (2024) Novel insights into Parkin–mediated mitochondrial dysfunction and "mito-inflammation" in α-synuclein toxicity. The role of the cGAS–STING signalling pathway. J Inflamm Res 17:4549–4574. https://doi.org/10.2147/JIR.S468609
84. Gonçalves FB, Morais VA (2021) PINK1: a bridge between mitochondria and Parkinson's disease. Life 11:371. https://doi.org/10.3390/life11050371
85. Basak B, Holzbaur ELF (2025) Mitophagy in neurons: mechanisms regulating mitochondrial turnover and neuronal homeostasis. J Mol Biol. https://doi.org/10.1016/j.jmb.2025.169161
86. Ammal Kaidery N, Thomas B (2018) Current perspective of mitochondrial biology in Parkinson's disease. Neurochem Int 117:91–113. https://doi.org/10.1016/j.neuint.2018.03.001
87. Lim K-L, Ng X-H, Grace LG-Y, Yao T-P (2012) Mitochondrial dynamics and Parkinson's disease: focus on Parkin. Antioxid Redox Signal 16:935–949. https://doi.org/10.1089/ars.2011.4105
88. Abu Shelbayeh O, Arroum T, Morris S, Busch KB (2023) PGC-1α is a master regulator of mitochondrial lifecycle and ROS stress response. Antioxidants 12:1075. https://doi.org/10.3390/antiox12051075
89. Chen L, Qin Y, Liu B et al (2022) PGC-1α-mediated mitochondrial quality control: molecular mechanisms and implications for heart failure. Front Cell Dev Biol. https://doi.org/10.3389/fcell.2022.871357
90. Azam S, Kim I-S, Choi D-K (2022) α-Synuclein upregulates bim-mediated apoptosis by negatively regulating endogenous GCN5. Aging Albany NY 14:8292–8301. https://doi.org/10.18632/aging.204353
91. Rius-Pérez S, Torres-Cuevas I, Millán I et al (2020) PGC-1 α, inflammation, and oxidative stress: an integrative view in metabolism. Oxid Med Cell Longev 2020:1–20. https://doi.org/10.1155/2020/1452696